Ivar Bratberg

Effect of the force distribution in dry granular materials

Presented in partial fulfillment of the requirements for the degree of Dr.Ing.

Dr.ing.-thesis 2003:113

Fakultet for informasjonsteknologi, matematikk og elektronikk
Institutt for Teleteknikk

NTNU

URN:NBN:no-3475

Effects of the force distribution in dry granular materials

Ivar Bratberg

A thesis in partial fulfilment of the requirements for the doctoral degree

Doktor Ingeniør

Department of Telecommunications
Norwegian University of Science and Technology
Trondheim, Norway

September 2003

URN:NBN:no-3475

URN:NBN:no-3475

Abstract

This work concentrates on the force-network of dry granular materials. The dynamical and static properties of the force-network are studied through simulations and experiments.

We study the structural properties of two-dimensional granular packings prepared by random deposition from a source line. We consider a class of random ballistic deposition models based on single-particle relaxation rules controlled by a critical angle, and show that these local rules can be formulated as rolling friction in the framework of dynamic methods for the simulation of granular materials. We find that the packing prepared by random deposition models is generically unstable, and undergoes dynamic rearrangements. As a result, the dynamic method leads systematically to a higher solid fraction than the geometrical model for the same critical angle. We characterise the structure of the packings generated by both methods in terms of solid fraction, contact connectivity and anisotropy. Our analysis provides evidence for four packing regimes as a function of solid fraction, the mechanisms of packing growth being different in each regime.

Using the Contact Dynamics method, the stick-slip response of an pushed granular column is analysed and a power law is found for the distribution of slips with exponent value 1.8. The exponent is invariable to perturbations of the different physical parameters. Two velocity regimes were found: stick-slip and steady state. These two regimes could be observed for very simple systems, making a detailed analyses possible.

An experiments on narrow granular columns to test the validity of the Janssen law under such conditions has been done. The weight at the bottom of the cylinder and the compression and movement of the packing have been measured. The apparent mass dependence on height is not in good agreement with the Janssen law using a one-parameter fit. A two-parameter fit yilded good results for the apparent mass during upwards and downwards movement at constant velocity of the granular column inside the enclosing cylinder. The necessity of two parameters has its origin in rotational frustration. The dependence of the apparent mass on the diameter of the column does not follow the Janssen law. Rather, it depends strongly on details of the packing.

URN:NBN:no-3475

.

URN:NBN:no-3475

Preface

This thesis is financed through a Strategic University Programme, funded by the Norwegian Research Council. The Department of Telecommunications, NTNU has provided additional support for fifteen months. This project has also gained support from CNRS (Centre National de la Recherche Scientifique), France, through the Franco-Norwegian PICS program, Grant No. 753. The thesis is a product of collaboration between Department of Petroleum Engineering & Applied Geophysics, NTNU; Department of Physics, NTNU; Department of Telecommunications, NTNU and SINTEF Petroleum Research. My formal position has been at the Department of Telecommunications. My supervisors have been Jens M. Hovem at department of Telecommunications and Alex Hansen at Department of Physics, NTNU. The subject of this thesis sorts under physics. A part of the work has been performed at Department of Physics in Oslo, with professor Knut Jørgen Måløy as an advisor. During the work I have had the pleasure of having a close cooperation with Frank Farhang Radjai at Centre National de Research Scientifiqe Montpellier, France. Kaarina has helped me improving my English. I would like to thank all the people mentioned above for their help and patience.

.

Papers

- Dynamic Rearrangements and packing regimes in Randomly Deposited Beds, I.Bratberg, F.Radjai, A. Hansen, *Phys.Rev. E.*, **66** (2002).
- Intermittent flow of a collection of rigid frictional disks in a vertical pipe, I. Bratberg, F. Radjai and A.Hansen, submitted to *Phys.Rev.E* February (2003).
- Validity of the Janssen law in narrow granular columns, I. Bratberg, K.J. Måløy, A. Hansen, submitted to *Phys. Rev. E*, September (2003).

.

Contents

1 Introduction

This thesis is about the properties of the force-network of dry granular materials. The main results of the research performed are presented in three papers. This introduction to the thesis will therefor give the theoretical framework for the papers. It is, among others, the complexity of the force-network which makes the field of granular materials such a rich one. The direct observation of the force-network is interesting itself, but the manifestation of it can be just as fruitful to study. One example of this is the stick-slip behaviour for granular material which is slowly sheared. Usually the correlation lengths are very long, and minor changes at one place can change the macroscopic properties of the material significantly.

The field of granular materials combines different classical fields like mechanics, material physics and statistical physics. One aim of the scientists of this field is to predict macroscopic properties from microscopic properties. It is an ongoing debate whether this will be possible, as it is not proved that fluctuations seen for small samples will disappear for larger samples. These facts open a possibility for numerical algorithms to play a crucial role in the study of granular materials. Quite simple rules implemented for the interactions between the particles can result in surprisingly complex macroscopic behaviour. For the simulations done in this thesis, a numerical model called the Contact Dynamics method [1, 2, 3] is used. It is a rather rapid algorithm. Even though the equations describing the friction and collision forces are simple, the numerous particle interactions give rise to a complex behaviour.

1.1 Background and motivation

One important feature of granular materials, as well as other materials, is the geometrical structure. Therefore it is of interest to try to model the creation of structures. One example is the modelling of sintering, another example can be the modelling of the filtering cake during filtration. Most algorithms developed so far have been purely geometrical due to the large number of particles involved. In the first paper of this thesis it is shown how Contact Dynamics can be used to develop more physical realistic models of packings. The combination of the Contact Dynamics' rather rapid execution together with the growth of computational power has made this field a mature one. The same Contact Dynamics program is used in the second paper to analyse the behaviour of a quasi-static pushed column of granular material. Interesting stick-slip patterns are seen, and the simulations allow us to study thoroughly different properties of the dynamics during the translation.

Many fundamental properties of the granular materials are poorly understood, and a quite simple experiment performed by pushing a column with equal-sized beads and measuring the force, has given quite surprisingly results. This is described in the third.

1.2 Organisation of the introductory section

The rest of the introductionary section shortly introduces the relevant theoretical background. In addition, short summaries of the papers are presented where they fit in. Chapter two presents the theory of packing of granular materials. Studies of the geometry of packings and algorithms for creating them are presented. The third chapter presents the properties of the force-network in granular materials and different theories explaining them. The fourth chapter presents different numerical models which are common in this field. As Contact Mechanics is used in two of the papers, this algorithm is described more in details. The fifth chapter focuses on the Stick-slip properties of granular materials, and Self-Organised Criticality is mentioned.

2 Packing of granular materials

In the first paper we present a method for creation of two-dimensional packings by using the Contact Dynamics algorithm. In the following some fundamental properties of packings are described.

2.1 Properties of packings

The structural properties of granular packings are many and complex, there are different ways of describing them. Here, I will mention a few properties and give their mathematical descriptions.

The solid fraction is defined as:

$$sf = \frac{Volume\ occupied\ by\ the\ grains}{Sample\ volume} \tag{1}$$

In two dimensions the most dense packing has a solid fraction equal to 0.906... and in three dimensions is it 0.74048....

When doing simulations on granular packings, it is possible to find the contact angle which is defined as the angle between the horizontal and the line defined by the centres of the two particles in contact. It is therefore of use to define a probability for a contact angle θ [4]. Let this probability expanded in a Fourier series with three terms around its principal axis:

$$P(\theta) = \frac{1}{2\pi}\left(1 + \gamma\cos(\theta - \theta_c) + A\cos(2[\theta - \theta_c])\right). \tag{2}$$

By claiming that $P(\theta)$ should have a period π, it is found that $\gamma = 0$, and we can write:

$$P(\theta) = \frac{1}{2\pi}\left(1 + A\cos(2[\theta - \theta_c])\right). \tag{3}$$

The contact angle tensor is written $\phi =< n_i^i n_i^j >$, where i is the contact number, and $i,\ j$ denotes the components of the normal vectors. Expanded into a matrix form, the tensor is written:

$$\phi = \frac{1}{c}\begin{bmatrix} \Sigma\cos^2\theta_i & \Sigma\sin\theta_i\cos\theta_i \\ \Sigma\sin\theta_i\cos\theta_i & \Sigma\sin^2\theta_i \end{bmatrix}, \tag{4}$$

where c is the number of contacts, and the sum goes over all the contacts. This tensor can be represented by an ellipse, with a major axis and a minor axis. If the axis are rotated an angle θ_c such that the $\Sigma\cos^2(\theta - \theta_c)$ term in the tensor is maximum, this defines the direction of the principal axis. In this case it follows from the properties of an ellipse, that the off diagonal terms are zero. Hence, by diagonalisation the tensor, the principal axis of the contact network are found.

An expression for A in eq. (3) can be found by putting in eq. (3) into the matrix and integrating over all angles. The result is:

$$\begin{pmatrix} \frac{1}{2}A\cos(\theta_c)^2 - \frac{1}{4}A + \frac{1}{2} & \frac{1}{2}A\sin(\theta_c)\cos(\theta_c) \\ \frac{1}{2}A\sin(\theta_c)\cos(\theta_c) & \frac{1}{2} - \frac{1}{2}A\cos(\theta_c)^2 + \frac{1}{4}A \end{pmatrix} \tag{5}$$

The eigenvalues of this matrix are:

$$\begin{cases} \lambda_1 = \frac{1}{2} + \frac{1}{4}A \\ \lambda_2 = \frac{1}{2} - \frac{1}{4}A. \end{cases} \tag{6}$$

We see that the measure of anisotropy is $A = 2 * (\lambda_1 - \lambda_2)$.

Another property of packing structures is the coordination number. This is the average number of contacts per particle. In two dimensions for mono-sized disks the maximum coordination number is six. A coordination number equal to six is equivalent to a perfect packing. Only small displacements in the structure can give a rapid decay in the coordination numbers. The correlation length of faults is very long for high coordination numbers [5]. For a a infinite chain of particles the coordinate number is equal to two.

Another property of the the packing is the *density-density* correlation function [6]. Given a particle at the origin (r=0), the probability for a particle to be at the position r is given by the density-density correlation function $G(\vec{r})$:

$$G(\vec{r}) =< \rho(0)\rho(\vec{r}) > \tag{7}$$

The Fourier transform of this function is the Structure factor $S(\vec{q})$ measured in diffraction experiments (light scattering, neutron scattering, electron diffraction etc.).

2.2 Packing structures

In two dimensions the most dense packing is the hexagonal packing as shown if Fig. 1. The solid fraction for this structure is:

$$sf = \frac{1}{2}\frac{\pi r^2}{\sqrt{3}r^2} = 0.9068... \tag{8}$$

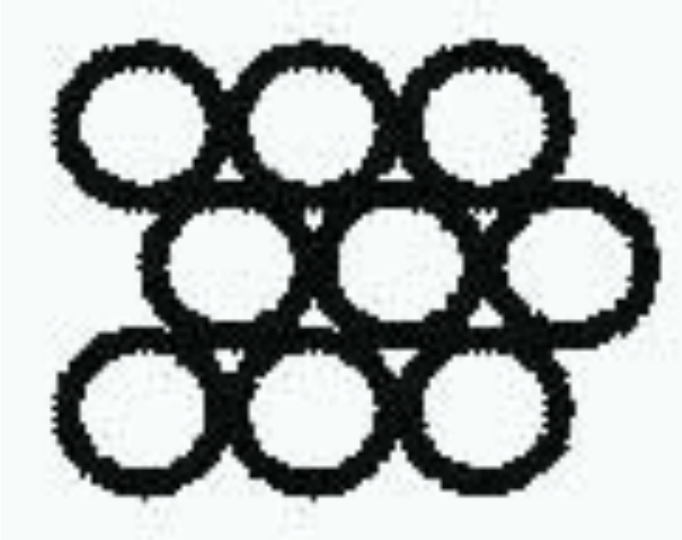

Figure 1: The most dense packing in 2D, the hexagonal packing. The solid fraction is 0.9068....

In three dimensions there are two structures with the maximum solid fraction for mono-sized beads. These are the body-centered cubic and the hexagonal closest packing, illustrated in Figs. 2 and 3.

However, the most dense packing structures are difficult to reach, unless the particles are manually set at their right position. Therefore another limit is defined, the Random Closest Packing (RCP). There is no exact definition of the Random Closest Packing. RCP is achieved when mono-sized beads are packed together and allowed to reorganise to achieve as close packing as possible. It is assumed that there are no walls restricting the packing. For two dimensions the solid fraction of RCP is found to be around 0.82 ± 0.005 [7]. The limit was found by the help of simulations, using a random deposition model. In three dimensions the solid fraction of RCP was found to be around 0.635 ± 0.0005 [8]. The solid fraction was found by filling up different-sized cylinders with mono-sized beads, and measuring the solid fraction. The solid fraction was then extrapolated and found for infinite cylinders. The Random Loose Packing (RLP) has not been studied

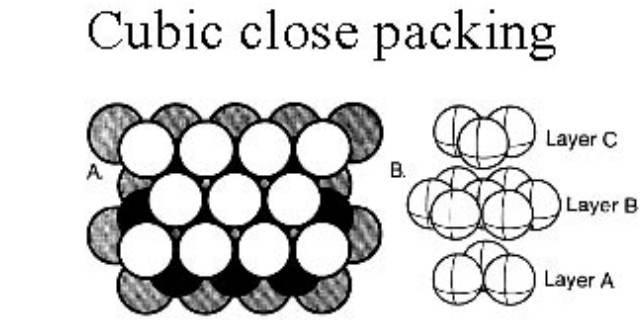

Figure 2: The cubic close packing. It can be formed by putting groups of three and three layers on the top of each other. All the three layers in one group have the same structure, but they are all displaced a little relative to each other. [9]

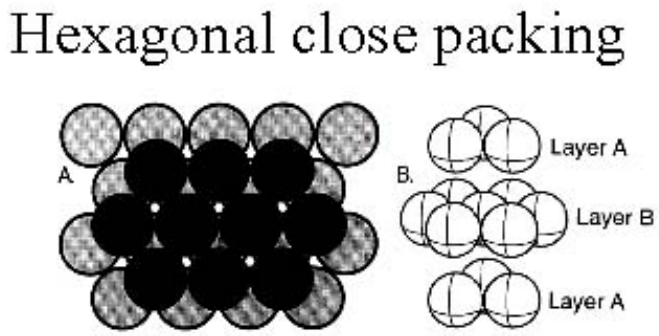

Figure 3: The hexagonal closest packing. It can be formed by putting groups of two and two layers on the top of each other. Each layer in the group has the same structure, but they are slightly displaced relative to each other. [9]

as extensively as the RCP limit. What is meant by RLP has not been well defined. A frequently used definition is the lowest stable packing solid fraction under external load. The smallest external load is the weight on the packing itself. Hence, the RLP limit depends on the gravity constant. This makes it reasonable to define the RLP in the limit when g goes towards zero. This limit has been measured experimentally to be $sf = 0.555$ [10] for 3D. These experiments were done by studying the densities of the packings which were immersed into liquids with different densities. The result was then found by extrapolating towards $g = 0$. In two dimensions this limit has been found using random deposition model, a simulation model. Beads are dropped onto a line and sticks on whatever it hits first, the line or an already deposited bead. It has been found in [7] at estimate of this limit: $sf = 0.3586 \pm 0.0001$.

2.3 Packing generating models

There are several models for the study of generation of random packings using hard particles and spheres. They have been used for the study of liquids [11] , amorphous materials [12], electrical conductivity [13], filtering and porous media [14], cohesive powders [15, 16, 17] and other mechanical properties.

The different models may be classified into two main categories:

- Those using only geometrical aspects of the particles and the packing environment.
- Those trying to model forces on and between the particles during the packing process.

Sequential models and collective reorganisation models must be sorted under the first category. The sequential models may again be divided into two sub-categories: In the first sub-category, particles are dropped one and one onto the packing structure, and following certain rules, remain stuck on the place where they first hit, or slide downwards until required condition is fulfilled [18]-[23]. In the other sub-category the particles grow around one center particle. [24]-[26]. For the method using collective reorganisation [27]-[34], the particles are first placed randomly in space. Second, a relaxation step follows, adjusting the diameters and the centres, until a stable configuration without overlap between the particles is achieved. Of the second main category few models exists, mainly due to the demand for computational power. Recently there have been some simulations done on packing where Van der Waals forces have been included.[15][16].

It is of high interest to be able to create packing of different porosities. Often a simple geometrical model like Random Ballistic Deposition has been used for this[17]. This is often good enough for some cases but no studies seem to exist of the differences between a geometrical model without dynamic rearrangementss, and a more physical complete model including this. With dynamic rearrangement is meant a rearrangment

of many particles in the packing due to the increased load during the packing process. It is of interest how the dynamic rearrangements influence on the properties of the packing. This is the aim of the first paper.

2.4 Using Contact Dynamics to study the two-dimension granular packings

In the first paper we study the structural properties of two-dimensional granular packings prepared by random deposition from a source line. We consider a class of random ballistic deposition models based on single-particle relaxation rules controlled by a critical angle, and we show that these local rules can be formulated as rolling friction in the framework of dynamic methods for the simulation of granular materials. We find that the packing prepared by random deposition models is generically unstable, and undergoes dynamic rearrangements. As a result, the dynamic method leads systematically to a higher solid fraction than the geometrical model for the same critical angle. We characterise the structure of the packings generated by both methods in terms of solid fraction, contact connectivity and anisotropy. Our analysis provides evidence for four packing regimes as a function of solid fraction, the mechanisms of packing growth being different in each regime.

3 The force-network in a granular media

In the second and third paper, the properties of the force-network of the granular material are studied. This section will give the reader an introduction to the different theories of the force-network in granular material, which will be necessary to understand the context and the idea behind the work presented in these papers. In Fig. 4 a visualisation of the forces in a granular packing can be seen [35]. There is a network of forces, or a collection of paths which carries forces. The amount of force carried by each of the paths varies. In Fig. 4*b* the distribution of forces between the contacts is shown. The visualisation of inter-granular forces was presented already in 1957 by Dantu [36]. It is widely believed that the existence of force chains is a major property of a granular material. There exists a range of theories which tries to explain this [35, 37, 38, 39, 40]. Numerical simulations have also been carried out, trying to recreate the force-network [41].

3.1 Continuum models

Even though the granular medias are a collection of discrete particles, it has been put an effort in trying to describe it as a continuum. The basic assumption is that there is a high correlation of the properties at a mesoscopic range making local averages valid

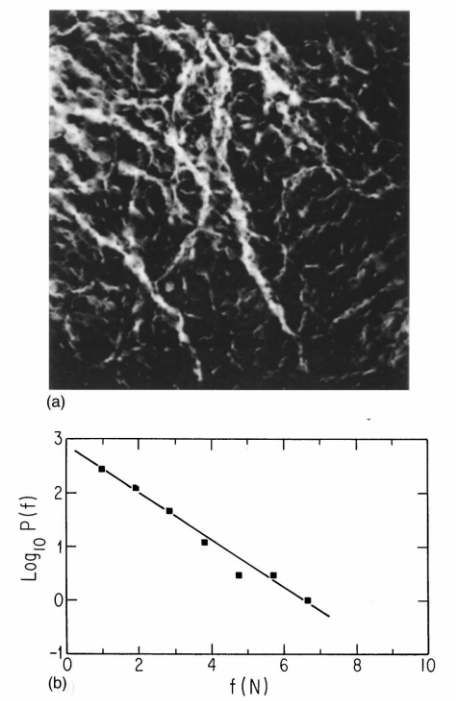

Figure 4: 3 mm Pyrex spheres are surrounded by a mixture of water and glycerol that matches the index of refraction of the Pyrex. A force is exerted on a piston that covers the top surface of the container. The stress-induced birefringence makes those beads under stress visible as the bright regions. The distribution of forces P versus force f were measured at the bottom of a cylindrical container filled with spheres. The bottom of the container was lined with carbon paper and a force was applied to the top surface. The line is an exponential fit to the data: $P(f) = \exp -f/f_0$. After Liu et al. (1995) [35] and [42].

and representative for the state of the bulk. This permits us to write up the equation of force balance using the stress tensor σ_{ij}. The stress tensor is an average of the contact forces in the neighbourhood.

3.1.1 The stress tensor

The stress tensor has two principal axis, the principal axis along where the principal stress propagates, and the minor axis along where the minimum stress propagates. The general stress tensor in 2D for axis x and $y \perp x$ may be written like:

$$\sigma_{ij} = \begin{bmatrix} \sigma_{xx} & \sigma_{yx} \\ \sigma_{xy} & \sigma_{yy} \end{bmatrix} \tag{9}$$

By imposing rotational equilibrium ,$\sigma_{xy} = \sigma_{yx}$, it is possible to represent the stress tensor by a what is called the stress quadratic. In two dimensions, this will take the form of an ellipse. Now, by changing the coordinate system to (m, n) which is rotated a certain angle compared to (x, y) it is possible to set $\sigma_{mn} = 0$. In other words, it is always possible to diagonolise the stress tensor by choosing the appropriate axis.

$$\sigma = \begin{bmatrix} \sigma_{mm} & 0 \\ 0 & \sigma_{nn} \end{bmatrix} \tag{10}$$

3.1.2 The Mohr Circle

Consider a box of granular media which has a vertical stress σ_v and horizontal stress σ_h, Fig. 5. No shear forces are working on the four side walls. Consider a plane inside the box at an angle α to the horizontal, see Fig. 6. The shear stress T_α and the normal stress σ_α are found imposing force equilibrium:

$$\sigma_\alpha = \sigma_h \sin^2 \alpha + \sigma_v \cos^2 \alpha \tag{11}$$

Through the relations $\cos^2 \alpha = (1 + \cos 2\alpha)/2$ and $\sin^2 \alpha = (1 - \cos 2\alpha)/2$ one gets:

$$\sigma_\alpha = \frac{\sigma_v + \sigma_h}{2} + \frac{\sigma_v - \sigma_h}{2} \cos(2\alpha) \tag{12}$$

$$\tau = \frac{\sigma_v - \sigma_h}{2} \sin(2\alpha)\,. \tag{13}$$

This equation is visualised by the Mohr Circle [43], Fig. 7. The first axis is σ_α, the second axis is τ_α. We can see that the shear stress is largest for $\alpha = 45°$.

The Coulomb criteria for slip for the plane α can be written:

$$|\tau_\alpha| > tan(\phi)\sigma_\alpha \tag{14}$$

This condition should hold for all angles in the granular media. This can be visualised by a straight line, see the bold dashed line in Fig. 7. If the line crosses the Mohr circle, there will be a slip. Through geometric considerations, see Fig. 7, the Coulomb criteria can be written:

$$\Upsilon \equiv \frac{R}{Psin\theta} \leq 1, \tag{15}$$

where R is the radii of the Mohr circle, and P is the horizontal displacement of the centre of the circle.

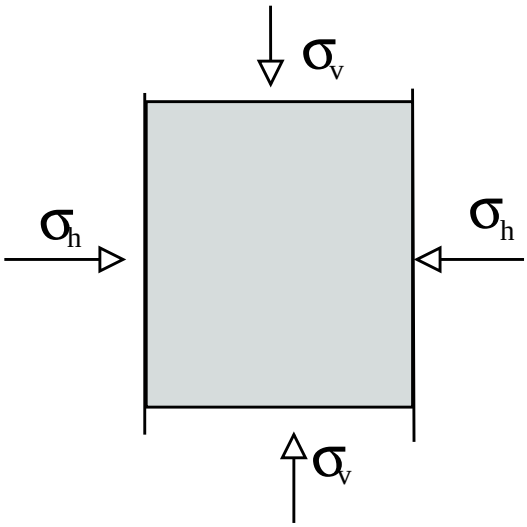

Figure 5: Illustration of the setup for the calculation of shear stress in bulk

3.1.3 The force balance in the continuum model

For equilibrium on a segment Δx, Δz gives the following equations:

$$\begin{aligned} \delta_z \sigma_{zz} + \delta_x \sigma_{xz} &= \rho g \\ \delta_z \sigma_{zx} + \delta_x \sigma_{xx} &= 0 \end{aligned} \tag{16}$$

where z is the vertical axis, x is the horizontal axis, ρ is the density of the granular media and g is the gravity. As already shown, the following symmetry property for the shear stress is:

$$\sigma_{zx} = \sigma_{xz}. \tag{17}$$

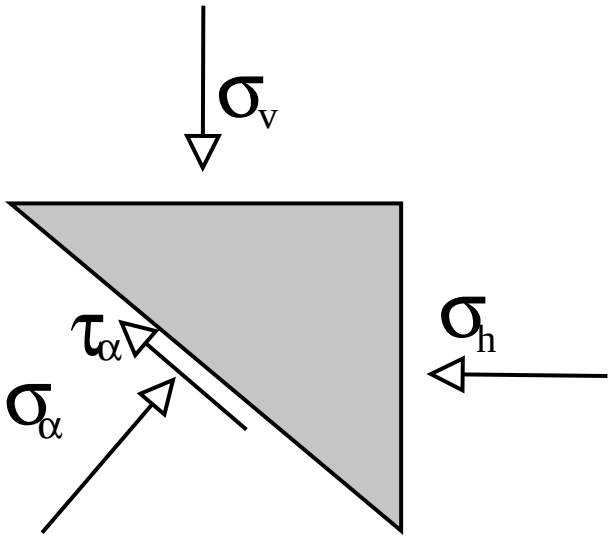

Figure 6: The normal- and shear-force working at a plane in the bulk

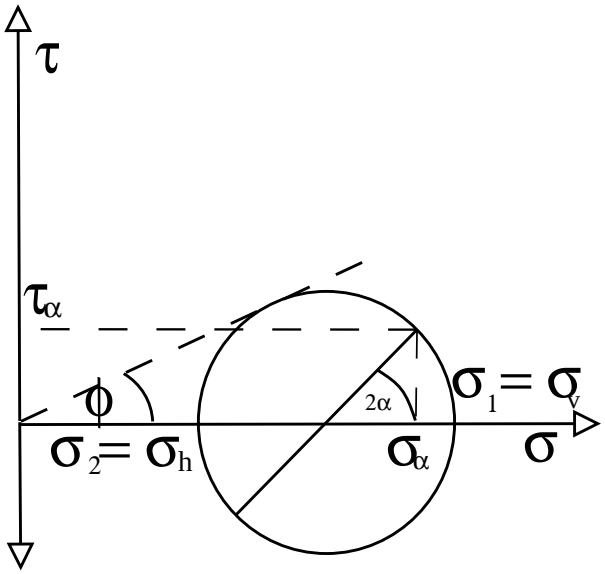

Figure 7: The Mohr stress circle, illustrating the normal and shear stress for a plane tilted an angle α relative to the active direction inside a bulk.

Now we have a system of three unknowns $\sigma_{xx},\ \sigma_{xz},\ \sigma_{zz}$, but only two equations. This problem can be resolved by introducing elasticity into the system. However, there are

many models which solve the systems in other ways by introducing constitutive laws between the components of the stress tensor. One example of this is the the assumption made by Janssen [44] as we will study in the following section.

3.1.4 The Janssen equation

In the experimental paper, (paper number three), the Janssen equation is tested for its validity for small systems, and for dynamic situations. In this section we will shortly go through the assumptions done by Janssen and present the results of the third paper.

The Janssen equation was found empirically and published in 1895 [44]. This equation is still used today when constructing silos[45, 46]. The theory is based on on the idea that the vertical stress is proportional to the horizontal stress.

The assumptions are:

- The granular material is considered as a continuum.
- The average pressure in the radial direction is proportional to longitudinal pressure:

$$\sigma_{22} = K\sigma_{11}, \tag{18}$$

  1 symbolise the vertical direction, and 2 the radial direction, K is a positive constant less than one.

- The contacts forces from the walls on the particles are pointing upwards and the friction force are at the Coulomb limit.

The forces are balanced in the vertical direction:

$$(\sigma_{11}^{+} - \sigma_{11}^{-})\pi D^2/4 + \pi D K\mu\sigma_{11}dz = \pi D^2 gc\rho dz/4, \tag{19}$$

where σ_{11}^{+} is the pressure under the horizontal layer, σ_{11}^{-} is the pressure over the layer, D is the diameter of the column, g is the gravitational constant, c is the solid fraction and ρ is the mass density of the beads. This is written for a column:

$$\frac{d\sigma_{11}}{dz}\frac{D}{4K\mu} + \sigma_{11} = \frac{D\rho cg}{4K\mu}. \tag{20}$$

We rearrange and get:

$$\frac{\frac{d\sigma_{11}}{dz}\frac{D}{4K\mu}}{\frac{g\rho cD}{4K\mu} - \sigma_{11}} = 1. \tag{21}$$

A integration is made from the top to the bottom assuming zero pressure at the top:

$$\ln\left(g\rho c\frac{D}{4K\mu}-\sigma_{11}(h)\right)-\ln\left(g\rho c\frac{D}{4K\mu}\right)=-h\frac{4K\mu}{D}, \tag{22}$$

which gives:

$$-\sigma_{11}(h)\frac{4K\mu}{Dg\rho c}+1=e^{-\frac{4k\mu}{D}h}, \tag{23}$$

isolating σ_{11}:

$$\sigma_{11}(h)=\frac{Dg\rho c}{4K\mu}\left(1-e^{-\frac{4K\mu}{D}h}\right). \tag{24}$$

The apparent mass after directing the contact force from the wall on the particles upwards is:

$$M_{app}=M_{app}^{\infty}\left(1-exp(-h/\lambda)\right), \tag{25}$$

where

$$M_{app}^{\infty}=\lambda\pi D^2gc\rho/4. \tag{26}$$

Here we have introduced the screenig length λ:

$$\lambda=D/4K\mu \tag{27}$$

For two dimensions it can be shown that:

$$\lambda=\frac{L}{2K\mu} \tag{28}$$

and

$$M_{app}^{\infty}=\lambda Lgc\rho \tag{29}$$

where L is the width of the two dimensional cylinder. In the third paper we describe an experiment which has been done to check the validity of the Janssen equation for small systems. We filled a vertical glass column with equal sized ball bearing beads. We measured the weight at the bottom of the cylinder, the compression and the movement of the packing meanwhile the packing was moved up and down. This allowed us to test the Janssen equation for a very small number of beads. The apparent weights' dependence of height was found not to give a satisfactory fit with the Janssen law. This may be explained by the discreteness of the system. Consider figure 8. There is only a finite number of points which are in contact with the cylinder wall. In the following we will derive equations for the force at the bottom of this setup assuming that the beads only slides upward along the wall due to rotational frustration.

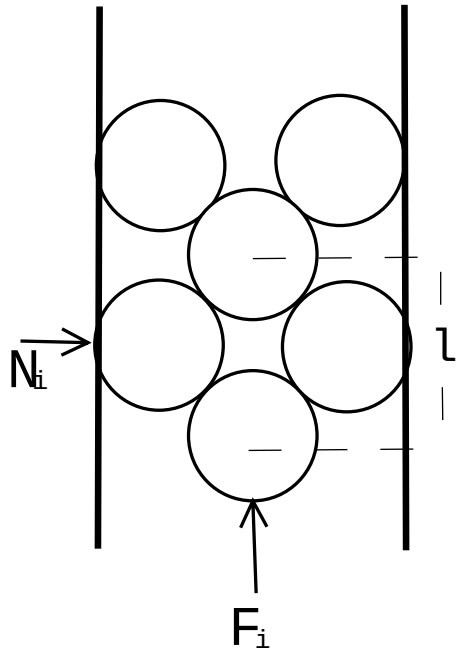

Figure 8: A two dimensional packing used for the derivation of an alternative to the Janssen equation. l is the height of one unit cell. In the derivation, the particles are supposed to not rotate due to rotational frustration.

Assume the coefficient of friction against the wall to be μ for all the bead-wall contacts. One unit cell in this structure is marked, and consists of one centered bead below two beads confined to the wall. The vertical force balance for one such cell is:

$$F_i = 2N_i\mu + 3w + F_{i-1}, \tag{30}$$

where F_i is the vertical force working upwards on the centered bead in unit cell i , w is the weight of one bead and N_i is the contact force between the wall and the confined particles in unit cell i. It is assumed that the contact force is the same on the left and right hand side. Now we introduce the Janssen equation for the discrete system:

$$N_i = KF_i, \tag{31}$$

where K is the Janssen coefficient. This gives:

$$F_i = 2F_iK\mu + 3w + F_{i-1}, \tag{32}$$

which can be rewritten as an discrete recursive equation:

$$F_i = AF_{i-1} + B \tag{33}$$

where $A = \frac{1}{1-2K\mu}$ and $B = \frac{3w}{1-2K\mu}$. We note that $F_0 = 0$. By substitution it can bee seen that:

$$F_{N-1} = B\Sigma_{i=0}^{i=N-1}A^i = B\frac{1-A^N}{1-A} \tag{34}$$

We subsitute back the physical parameters:

$$\frac{1}{1-A} = \frac{3w}{1-2K\mu-1} = -\frac{3w}{2K\mu} = -\frac{3g\rho S/}{2K\mu}, \tag{35}$$

where ρ is the mass density of the beads, S is the volume of one bead, and g is the gravitational constant. Now we introduce the solid fraction for a unit cell c, and the width of the cylinder l and the height of one unit cell l, which allows us to write

$$\frac{1}{1-A} = -\frac{\rho cglL}{2K\mu} \tag{36}$$

The height h is given by $h = Nl$. We rewrite the exponential:

$$A^N = \exp(\ln(A^N)) = \exp(h/l\ln A), \tag{37}$$

and get:

$$F_i = \lambda_1\rho cL\left(1-\exp(-h/\lambda_2)\right), \tag{38}$$

where

$$\lambda_1 = -\frac{l}{2K\mu}, \tag{39}$$

and

$$\lambda_2 = -l/\ln\left(\frac{1}{1-2K\mu}\right) \tag{40}$$

As an example we find for $K\mu = 0.1$ gives $\lambda_1/\lambda_2 = 1.1$. We conclude that the discrete model gives a different equation than the continuous case, and that for small systems this could be important. In the experiments we find that λ_1 is alwas larger than λ_2, which is in accordance with this theory.

3.1.5 The Oriented Stress Linearity (OSL) models

A central model for force distribution in granular materials is the OSL (Oriented Stress Linearity) model [37]. This model represents an attempt to explain the screening of forces which has been seen in both cylindric packings and piles. Many experiments have measured the hydrostatic pressure at the bottom surface of a pile. It has been reported that the stress at the centre is lower than the one further out [47]. A dip in the pressure is seen at the centre.

Here we will present the OSL model: Consider Fig. 9. A pile of sand is illustrated. The slope of the pile is ϕ. The stress lines in the model are directed along the vector $\mathbf{m}$, defined by the angle ψ. The normal vector of this is $\mathbf{n}$. The direction of the stress lines can vary with the position. The shear stresses along these lines are set to be limited by the following rule:

$$\sigma_{nn} = K\sigma_{mm}. \tag{41}$$

Equation (41) can be written in the Cartesian coordinate system:

$$\sigma_{xx} = \eta\sigma_{zz} + sign(x)\mu\sigma_{xz}. \tag{42}$$

The *sign* function is due to the discontinuous change at the symmetry axis in the stress function. By combining the static equilibrium equations (16) with the assumption in equation (41) and the symmetry condition eq.(17), it is possible to formulate a wave equation.

$$(\delta_z + c_+\delta_x)(\delta_z + c_-\delta_x)\sigma_{ij} = 0. \tag{43}$$

This is an hyperbolic wave equation which has two directions of propagation. The directions are given by the equations $x - c_+z$ and $x - c_-z$. The depth parameter z has the role of time in this wave equation. One direction of propagation is outwards, giving rise to the arching effect. The other direction is inwards.

Three other important assumptions in the OSL model are:

- The macroscopic properties of the granular medium are independent of length scale. This makes it possible to write:

$$\sigma_{mn} = \sigma_{mn}(z/Z, x/cZ), \tag{44}$$

  where c = cotan ψ, see Fig. 9, and Z is the height of the pile. Hence, it is convenient to use the reduced radius: $S = x/cZ$.

- The unknown stresses in chunks of material element only depend on the known stresses in that element. This makes it possible to write:

$$\sigma_{xx}/\sigma_{zz} = C(\sigma_{xz}/\sigma_{zz}, S) \tag{45}$$

- A principle called *perfect memory* is introduced. It is assumed that the constitutive relations do not change with time. At once a chunk of material is deposited at the surface of the pile, the relations between the stresses are set. This is at the surface, so the parameter S is equal to one. As the pile is growing, S for the same chunk of material is decreasing. Hence, for the assumption of *perfect memory* to be valid, the function C must be independent of S:

$$\sigma_{xx}/\sigma_{zz} = C(\sigma_{xz}/\sigma_{zz}) \tag{46}$$

The FPA model postulates that the major principal axis of the stress tensor has a fixed angle of inclination to the downward vertical:$\psi(x) = \psi_b$. The thought direction of the stress lines is defined forever in the moment the material is deposited at the surface of the pile. By assuming that the stress goes towards zero when approaching the surface, and using Mohr-Coulombs equation eq. (14), it is found that the angle of the principal axis in the stress tensor must be: $\psi_b = (\pi - 2\phi)/4$. Since the FPA model assumes that ψ is a constant, this is the direction of the principal axis for the whole bulk. The FPA is a special case of the OSL model. As already mentioned, the hydrostatic pressure on the bottom surface of a pile of granular materials has been measured. It is often found that there is a minimum of the pressure in the middle of the surface, and the maximum is localised on a ring around the centre. This surprising result can be explained by the FPA theory. The forces from the mass in the centre are carried away by stress lines pointing outwards, away from the centre line of the pile.

Another special case of the OSL theory is the so called BCC model [48]. The name is after the authors Bouchaud, Cates and Claudin. This assumes that there is a constant relation between the radial stress and the vertical stress:

$$\frac{\sigma_{xx}}{\sigma_{zz}} = \eta \tag{47}$$

It is easy to see that this is a special case of the OSL theory, when compared to equation (42).

This is related to the work of Janssen [44] who assumed that the stress tensor was only a function of the depth, and that the vertical stress was proportional to the horizontal stress The difference between these two theories is that the stress tensor in eq.(47) for the BCC model is also a function of the horizontal position: $\sigma = \sigma(z, r)$, while for Janssen $\sigma = \sigma(z)$.

Another special case is the IFE (Implicit Failure Everywhere). The IFE theory assumes that the bulk is at the Coulomb point all the time. This is expressed mathematically by setting $\Upsilon = 1$ in equation (15). Fig. 10 illustrates the calculation of the stress under a pile for the different special cases mentioned. It is shown that the FPA model is the only one that manages to recreate minimum property in the centre of the surface.

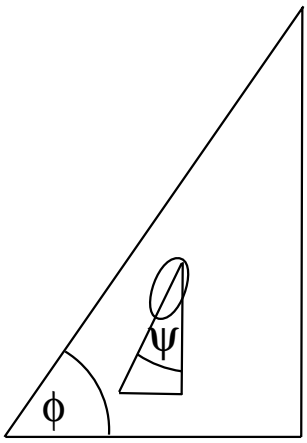

Figure 9: An illustration of the Oriented Stress Lines model. The parameter Ψ represents the orientation of the principal axis of the stress tensor while ϕ is the slope of the surface of the pile. The stress tensor is represented by the ellipse, with major axis along the angle ψ. The direction of the principal axis is a function of position.

3.2 The quasi-elastic model

Evesque and de Gennes[49] have suggested a theory based on what they call a quasi-elastic principle. It is inspired by a experiment done by Boutreux [50]. He studied avalanches in a silo where sand was poured from a small slit. The final slope of the pile was found always to be below the critical point where the sand is just about to flow. Hence, there should be no instability in the shear, and the sample should be under

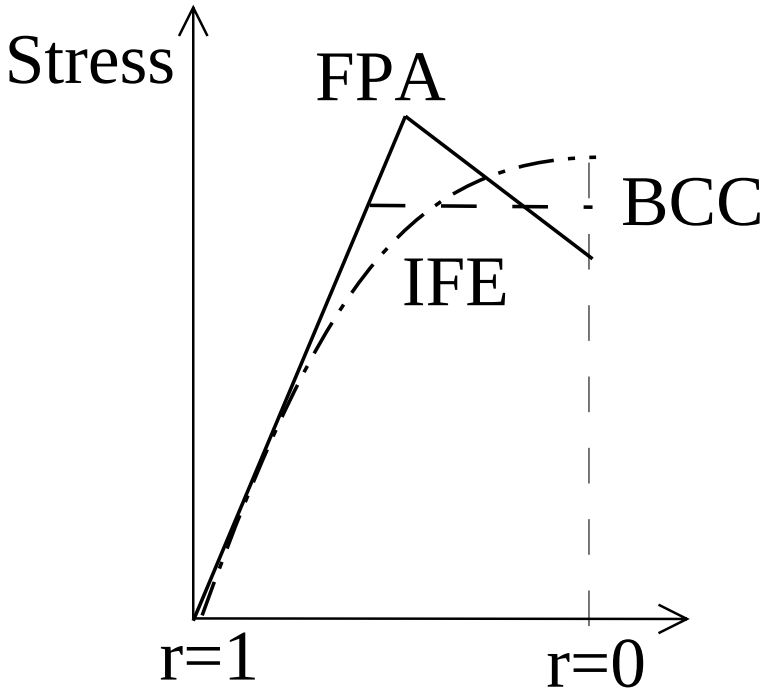

Figure 10: The stresses for the different models inside the OSL model. It should be noted that the FPA (Fixed Principal Axis) is the only one that recreates the minimum property of the stress field in the centre of the bottom surface.

compression everywhere. Experiments [51] have shown that for a granular material a macroscopic bulk modulus can be defined, and is shown to be around $K \propto p^{1/2}$, where p is the hydrostatic pressure. The increasing bulk with the pressure is due to the increased contact surface between the particles. For two spheres and Herztian contacts the modulus is expected to be $K \propto p^{1/3}$. In the quasi-elastic theory the columns are supposed to collapse under their own weight, creating a continuous displacement field. By taking into account the whole sample history and assuming a smaller displacement near the walls, they come up with a Janssen equation where the k_j is dependent of the Poisson ration ρ_p of the material:

$$k_j = \frac{\sigma_p}{1 - \sigma_p}. \tag{48}$$

Provided that σ_p is independent of the pressure, this supports the Janssen equation.

3.3 Critique of the models

The FPA model has received critique from Savage [52, 53] and Goddard [54]. The following summary of the article is based on the review paper of de Gennes[40]. The FPA model is based on the following assumption of what is happening during the filling of a container: as the particles fall into a 2D box they will form a slope $\tan\theta_s$. The relation between the shear stress and the normal stress on the surface can be written.

$$\tau = \sigma_n \tan\theta_s. \tag{49}$$

Now it is assumed that this relation also holds when the piles are covered of other layers of grain. Once buried, the stresses and the structure freeze. This model recreates the dip which has been observed under a pile. Savage claims the three following points:

- For two-dimensional heaps ("wedges") with a rigid support plane, there is no dip in the experiment.
- If the support is (very slightly) deformable, the stress field changes deeply, and a dip occurs.
- For the 3D case ("cones"), the results are extremely sensitive to the details of the deposition procedure.

Savages has also done a finite-element calculation where the inner part of the pile is seen as quasi-elastic and the surface is set to obey the Mohr-Coulomb conditions. With a rigid support no dip is found, while for an deformable support he finds a dip.

As an answer to this critics Cates claims that there is always a chance for some particle contact forces to be at critical point. Hence it is not assured that it is possible to define a bulk compressibility.

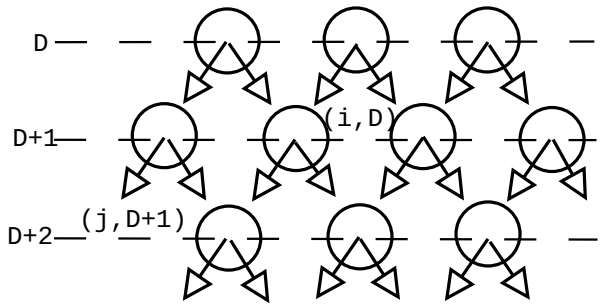

Figure 11: Illustration of the two-dimensional q-model. The particles in the D layer distribute the forces to their neighbours in the $D+1$ layer.

De Gennes responds to this by saying that shear test can be done, the bulk compressibility can be defined [40].

As a summary of the debate we see that there is on one hand a classical picture of the granular material which claims that the material can be described by continious elastic equations, and on the other hand a modern picture which claims that the critical state governs the properties.

3.4 q-model

Liu and co-workers [35] have presented a model, the q-model, where the vertical forces are spread from one particle to the particles below. The model was developed further by Coppersmith and co-workers [39]. In general, see Fig. 11, the equation of forces may be written:

$$w(j, D+1) = 1 + \Sigma_i q_{ij}(D) w(i, D), \tag{50}$$

where $w(j, D+1)$ is the weight on the bead in column j and row $D+1$, q_{ij} is the part of vertical force transmitted from the bead in column i to the bead in column j. The tensor q_{ij} is assumed to be independent of the row number. The conservation of forces gives:

$$\Sigma q_{ij} = 1 \tag{51}$$

In the most simple case in 2D, one particle transmits half of its vertical force plus its own weight to each of the two neighbours below. In more refined models the coefficients of force transmission q_{ij} can be represented by distributions. The q distribution must reflect the disorder of the packing. Consequently, even for a regular crystal, very complex force-networks can be modelled.

4 Numerical models

The first and second paper use Contact Dynamics to simulate granular materials. In this section the mathematical basis for the Contact Dynamics method is presented. Other numerical methods widely used to simulate granular materials are also presented.

4.1 Hard spheres

There are several regimes which are interesting to simulate. Some regimes are believed to be little influenced by elastic effects. The collisions are often described by the help of restitutional coefficients, which describe the relation between the impulses before and after a collision. Hence, the hard sphere term also includes elastic balls, as long as the kinetics of the system is the governing factor. Typically this is a system with a quite long mean free distance. In this regime it is popular to use event-driven algorithms or Contact Dynamics. In this category one should also add the geometrical algorithms used for constructing large packings.

4.2 Soft spheres

In the soft sphere regimes, the interaction force depends on the penetration length, and the particles have a low mean free distance. In some setups it is almost the same contact network throughout the whole simulation. Here the important physics is in the penetration effects. Molecular Dynamics is a popular tool in this regime.

4.3 The evolution of time

One question when doing numerics is what is the most rational way to split up the time. The answer to this must be the method which manages with least iterations in coming from time t_0 to time t_1. Hence, if a system is easily extrapolated in time, except for at certain events, the event driven algorithm is a good choice. The idea is to calculate the values of the system only for the events. Typically for a granular media this would be change of direction of one sliding contact, the breakage of one contact, the creation of one contact, a collision or a transition of one contact between sliding and non-sliding status. The event-driven algorithm will certainly work best for systems with a low rate of events. When the number of events become too high, numerical tricks must be done to avoid slow progress in the simulation.

4.4 Molecular Dynamics

Molecular dynamics is an extensively used method in many branches of science and engineering. There exists a large body of theory and a lot of software for this method,

and is comfortable to use as such. The time is divided into equal time steps, and for each time step the physical parameters are calculated. This can be written:

$$\Delta p = \Delta(mv) = mv - mv_0 = \int_0^{t_c} F_{cm} dt, \tag{52}$$

and

$$\Delta(I\omega) = I\omega - I\omega_0 = \int_0^{t_c} (r \times F) dt, \tag{53}$$

where I is the moment of inertia, $r \times F$ is the torque on the particle, ω is angular velocity, m s the mass of the particle, F_{cm} is the force at the centre of mass,v is the velocity f the particle and p is the impulse of the particles.

The elastic forces as a function of penetration are of major importance when simulating a particle system using MD. This is an active field of research. It is a complex task to define the contact forces during a collision, and approximations must always be done.

4.5 Collision models in MD

As already mentioned the physics of colliding spheres is hard to grasp and numerical models are based on approximations. For two overlapping spheres, it is of interest to find the force due to the overlap. A simple approximation is to assume a linear spring:

$$F_r = kd, \tag{54}$$

where F_r is the restitutional force, k is the spring constant, and d is the overlap. However Herzts law is assumed to be a more realistic model:

$$F_r = kd^{3/2}. \tag{55}$$

This is a very common assumption in the simulation of granular materials, and specially for the propagation of sound in granular materials. A simple derivation is proposed by de Gennes. Assume that the volume represented by the calott defined by the overlap h is compressed, and assume $h << R$ where R is the radius of the sphere. The area illustrated in Fig. 12 is proportional to $2Rh$. Next it is assumed that the depth of the sphere which is influenced by the overlap, is the same as the radii of the contacts circle, $\sqrt{2Rh}$. Using Youngs modulus the force is found:

$$F \approx AE\frac{h}{\sqrt{Rh}} = E\sqrt{(2R)}h^{3/2}. \tag{56}$$

Hertz law is an elastic model which does not loose energy during the collision. To introduce dissipation, different models can be used. One of the simplest models is to

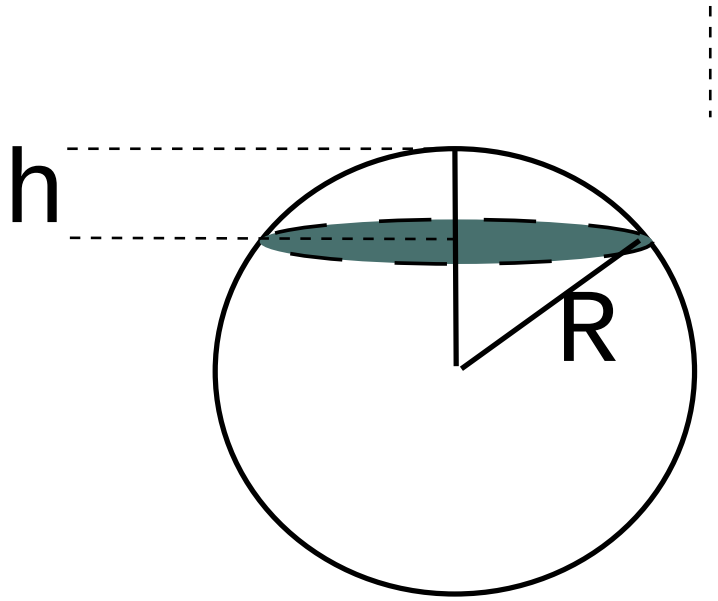

Figure 12: Illustration of the geometry for a collision. A basis for understanding the Hertz equation.

assume a viscous force proportional to the relative velocities. This dissipative force can be split into one normal component and one tangential component:

$$f_n^d = -d_n * m^{ij} v_n^{ij}, \tag{57}$$

and

$$f_t^d = -d_t * m^{ij} v_t^{ij}, \tag{58}$$

where m_{ij} is the reduced mass, i,j are the two particles, v_t is the tangential velocity and v_n is the normal velocity. Experiments have shown that for partially elastic collision, the rate of energy in the two particles before and after the collision can be written in terms of an restitutional coefficient:

$$\epsilon = \sqrt{(\frac{E_1}{E_0})}, \tag{59}$$

where E_0 and E_1 are the kinetic energy of the two particles [55] before and after a collision. The restitutional coefficient should be independent of the velocity and the initial separation between the particles. However, for very close initial separation, less than the penetration depth, the effective restitutional coefficient will be too large. The collision will be simulated more elastically than what it really is. This problem is called

the detachment effect, and shows that the method has problems in the regime of dense ensembles.

4.6 The Contact Dynamics algorithm

This algorithm was developed by Moreau and Jean [1, 2, 3]. The time is divided into equal intervals. The dynamic of each particle is characterised by the velocity of the centre and the rotational velocity. For each time step, the algorithm finds the pairs of particles which will collide in the next time step. The particles which overlap define the contacts of the system. Each contact is described by a normal force impulse, a tangential force impulse and a spin transfer. The collisions are described through restitutional coefficients. In the following sections I will describe the mathematical modelling of the collisions as it is used in this algorithm.

4.6.1 Modelling of frontal collisions

For two particles which collide and have no tangential relative velocity, a total elastic collision is written:

$$v_{ij}^{+} = -v_{ij}^{-}, \tag{60}$$

where the v_{ij}^{+} is the relative velocity after the collision and v_{ij}^{-} is the relative velocity before the collision. During the collision there is almost always some energy loss. Some loss may be due to plastic deformation, and some due to generation of vibrations in the packing. For non-elastic collisions experiments have shown that it is possible to write:

$$v_{ij}^{+} = -\rho_n v_{ij}^{-} \tag{61}$$

where ρ_n is Newtons restitutional coefficient. The velocities after the collisions can be found by using the equations:

$$m_i v_i^{+} = m_i v_i^{-} + R, \tag{62}$$

and

$$m_j v_j^{+} = m_j v_j^{-} - R, \tag{63}$$

where R is the impulse transfer during the collision. Now there are three equations with three unknowns. The relative energy loss for a collision ΔE can be calculated:

$$\frac{\Delta E}{E} = 1 - \rho_n^2, \tag{64}$$

where E is the energy before collision. What appears, is that ρ_n is a measure of the relative energy dissipation for a collision.

A tangential restitutional coefficient is used for collisions where there is also a relative tangential velocity. It takes the form:

$$v_{ij}^{t+} = -\rho_t v_{ij}^{t-} \tag{65}$$

where ρ_t is the tangential restitutional coefficient, v_{ij}^{t+} and v_{ij}^{t-} is the relative tangential velocity of the contact point after and before the collision. This is also an empiric law and should be used carefully. The restitutional coefficient ρ_t can be both negative and positive. During a collision the particles will either slide and/or roll against each other. The ρ_t should be connected to the frictional loss, and the elastic effect during the collision. This raises the question how the Coulomb laws for friction should be connected to this restitutional equation. We will come back to this later.

4.6.2 The normal force and the Signorini graph

The Signorini equation gives us the normal force as a functon of the overlap between two particles. For the Contact Dynamics method it is necessary to adopt a similare concept, but as we will see the Signorini condition is not sufficient. To get an easy start, let us consider only the normal forces. The normal force moments working on the particles i and j during a time step gives a change in the velocity:

$$v_i^{n+} - v_i^{n-} = \sum_{k \neq j} \frac{R_{ik}\hat{n}_{ij}\hat{n}_{ik}}{m_i} + \frac{R_{ij}}{m_i} \tag{66}$$

and

$$v_j^{n+} - v_j^{n-} = \sum_{l \neq i} \frac{R_{jl}\hat{n}_{ji}\hat{n}_{jl}}{m_j} - \frac{R_{ij}}{m_j}, \tag{67}$$

where $\hat{n}_{ij}$ is the normal unity vector pointing from the contact point between particle i and particle j towards the centre of particle i, m is the mass of the particle, R_{ij} the normal force moment transfer from neighbour j on i. The normal velocity is defined:

$$v_i^{n+/-} = (\vec{v}_i^{+/-})\hat{n}_{ij}, \tag{68}$$

where $\vec{v}_i$ is the velocity vector of one particle, and $\hat{n}_{ij}$ is the normal vector between the particles marked i and j. The plus and minus sign are marks for the time after and before the time elapse dt. Assuming N particles and C contacts and N equations of the type (66), we need C equations more, and these equations are the restitutional equations, eq. (61). Now there are enough equations. In the CD method, for each contact, R_{ij} is calculated from equations (66,67).

$$R_{ij} = m_{ij}^n \left((v_{ij}^{n+} - v_{ij}^{n-} - \sum_{k \neq j} \frac{R_{ik}\hat{n}_{ij}\hat{n}_{ik}}{m_i} + \sum_{l \neq i} \frac{R_{jl}\hat{n}_{ji}\hat{n}_{jl}}{m_j} \right) \tag{69}$$

where

$$\frac{1}{m_{ij}^n} = \frac{1}{m_i} + \frac{1}{m_j}. \tag{70}$$

It might happen that R_{ij} comes out negative, which indicates that there is no collision, equation (61) is not valid anymore. What we need, is a new definition of the term contact for the calculations. Even if two particles are geometrically in contact, it might happen that the contact is not transmitting force. A parallel to the Signorinis law is introduced. The Signorinis law is a relation between the distance between two particles and the interstitial force:

$$\begin{cases} d = 0 & \Rightarrow \quad R > 0 \\ d > 0 & \Rightarrow \quad R = 0 \end{cases} \tag{71}$$

where d is the distance between the two contact surfaces, and R normal opposing force between the two particles. In our case, we must instead use:

$$\begin{cases} R > 0 & \Rightarrow \quad R > 0 \\ R <= 0 & \Rightarrow \quad R = 0 \end{cases} \tag{72}$$

In practise it means that if a normal force is calculated to be negative, the contact is removed from the set of equations. To express this non-smooth limitation in a diagram similar to a Signorini graph, we may introduce a formal velocity $\bar{v}_{ij}^n$:

$$\bar{v}_{ij}^n = v_{ij}^{n+} + \rho_n v_{ij}^{n-} \tag{73}$$

Now we may express the new Signorini condition as follows:

$$\begin{cases} \bar{v}_{ij} = 0 \Rightarrow \ R_{ij} \geq 0 \\ \bar{v}_{ij} \neq 0 \Rightarrow \ R_{ij} = 0 \end{cases} \tag{74}$$

We can rewrite equation (69) using the normalised velocity:

$$R_{ij} = m_{ij}^n \bar{v}_{ij} + K_{ij}, \tag{75}$$

where

$$K_{ij} = m_{ij}^n \left(-\sum_{k \neq j} \frac{R_{ik}\hat{n}_{ij}\hat{n}_{ik}}{m_i} + \sum_{l \neq i} \frac{R_{jl}\hat{n}_{ji}\hat{n}_{jl}}{m_j} - v_{ij}^{-}(1 + \rho_n) \right) \tag{76}$$

In figure(14) we have plotted the force moment as a function of the formal velocity. The bold line represents the condition expressed in equation(74). The axis along the formal velocity represents different relations between the velocities. Only for $\bar{v} = 0$ the relation correspond to the restitutional relations.

4.6.3 The tangential velocities

Now we introduce the tangential velocities during the collisions. As mentioned, the relations between the tangential velocities before and after the collisions are described by restitutional equations as well. The equations for the change of the tangential velocity during a time step are:

$$(v_i^{t+} - v_i^{t-})m_i = \sum_k T_{ik}\hat{t}_{ij}\hat{t}_{ik} + \sum_k R_{ik}\hat{t}_{ij}\hat{n}_{ik} + \sum_k T_{ik}\frac{r_i^2}{I_i} \tag{77}$$

and

$$(v_j^{t+} - v_j^{t-})m_j = \sum_l T_{jl}\hat{t}_{ji}\hat{t}_{jl} + \sum_l R_{jl}\hat{t}_{ji}\hat{n}_{jl} + \sum_l T_{jl}\frac{r_j^2}{I_j}, \tag{78}$$

where $\hat{t}_{ij}$ is the tangential unity vector in the contact between particle i and j pointing in the counterclockwise direction. I_i and I_j are the moments of inertia. T_{ij} is the tangential force moment during the collision. Using the tangential restitutional equation, we isolate T_{ij} and $T_{ji} = -T_{ij}$ by subtracting the equations from each other:

$$\begin{aligned} T_{ij} = m_{ij}^t \Bigg(& v_{ij}^{t+} - v_{ij}^{t-} - \frac{\sum_{k\neq j} T_{ik}\hat{t}_{ij}\hat{t}_{ik}}{m_i} + \frac{\sum_{l\neq i} T_{jl}\hat{t}_{ji}\hat{n}_{jl}}{m_j} \\ & - \frac{\sum_k R_{ik}\hat{n}_{ij}\hat{n}_{ik}}{m_i} + \frac{\sum_l R_{jl}}{m_j}\hat{n}_{ij}\hat{n}_{jl} - \frac{\sum_{k\neq j} T_{ik}\frac{r_i^2}{I_i}}{m_i} + \frac{\sum_{l\neq i} T_{jl}\frac{r_j^2}{I_j}}{m_j} \Bigg) \end{aligned} \tag{79}$$

where

$$\frac{1}{m_{ij}^t} = \frac{1}{m_i} + \frac{1}{m_j} + \frac{r_i^2}{I_i} + \frac{r_j^2}{I_j} \tag{80}$$

We may write equation(79) as an equation with one velocity dependent term and one force moment dependent term:

$$T_{ij} = \bar{v}_{ij}^t m_{ij}^t + L_{ij}. \tag{81}$$

where we have defined the tangential formal relative velocity as:

$$\bar{v}_{ij}^t = v_{ij}^{t+} + \rho_t v_{ij}^{t-} \tag{82}$$

and L_{ij} is:

$$\begin{aligned} L_{ij} = m_{ij}^t \Bigg(& -\frac{\sum_{k\neq j} T_{ik}\hat{t}_{ij}\hat{t}_{ik}}{m_i} + \frac{\sum_{l\neq i} T_{jl}\hat{t}_{ji}\hat{n}_{jl}}{m_j} \\ & -\frac{\sum_k R_{ik}\hat{n}_{ij}\hat{n}_{ik}}{m_i} + \frac{\sum_l R_{jl}}{m_j}\hat{n}_{ij}\hat{n}_{jl} - \frac{\sum_{k\neq j} T_{ik}\frac{r_i^2}{I_i}}{m_i} + \frac{\sum_{l\neq i} T_{jl}\frac{r_j^2}{I_j}}{m_j} - v_{ij}^{t-}(1+\rho_t) \Bigg) \end{aligned} \tag{83}$$

4.6.4 Coulomb law

The equation above is valid if the tangential restitutional equation (61) is valid. However, if $|T_{ij}|$ is large enough, one would expect the restitutional equation to become unvalid because the two particles would then only slide against each other during the collision obeying a Coulombian friction law. The mechanics during a collision is complicated, but as an approximation, the following extended Coulomb rule is used for the CD program.

$$\begin{cases} \mu R_{ij} > |T_{ij}| \rightarrow \text{ Sliding} \\ \mu R_{ij} <= |T_{ij}| \rightarrow \text{ Non Sliding} , \end{cases} \tag{84}$$

where μ is the friction coefficient. This equation is reasonable as it is the relation you will get assuming Coulombs criteria valid for all the time during the collision, integrating the terms in the Coulombs criteria over the collision period. Equation(79) holds only as long as the tangential restitutional equations hold. To be able to draw the non-smooth equation (84) as a function of one parameter, the formal tangential velocity as defined in equation (82) is used. Note that the equation (84) is only valid for $\bar{v}_t = 0$. The formal tangential velocity is a measure of the relation between the relative velocities before and after a time step, and only when it is equal to zero this relation is equivalent to the restitutional equation. Hence, when $v_{ij}^t \neq 0$ we must have $T_{ij} = sign(v_{ij}^t)\mu R_{ij}$. We also need to know what the sign of $\bar{v}_{ij}^t$ means for the sign of T_{ij}. So far we only know the amplitude. Assume $v_{ij}^- = v_i^- - v_j^- > 0$, and assume $\rho_t > 0$. The T_{ij} for the time step is negative as long as the restitutional coefficient holds, because $v_{ij}^+ < 0$. If the magnitude of T_{ij} is calculated to be larger than the Coulombian friction limit μR_{ij}, the magnitude of T_{ij} must be decreased and the new value be set to $-\mu R_{ij}$. This means that the new calculated v_{ij}^+ will be less negative. This again implies that $\bar{T}_{ij}^t = v_{ij}^+ + \rho_t v_{ij}^- > 0$ will go positive. Likewise we can analyse when $T_{ij} > 0$. The arrows in figure 13 illustrates this analyses. If T_{ij} is outside the Coulomb limit, it will be mapped as the arrows indicates onto the bold line. The crossing between the straight line and the stair-case like line gives us the correct value of T_{ij}. This graph also indicates that there will be one unique solution.

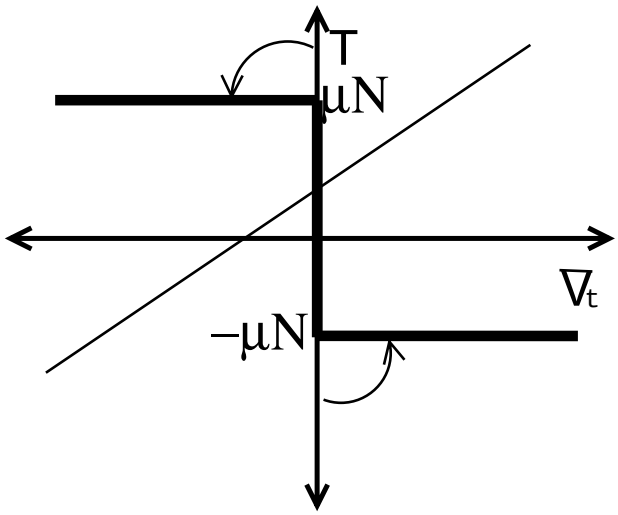

Figure 13: The Coulomb graph and the tangential force moment transfer as a function of the tangential normalised velocity, $\bar{v}_t$. If $\bar{v}_t \neq 0$, we are outside the Coulomb limit, the tangential force moment during the collision must be $T = \pm\mu R$. If we are inside the Coulombs limit the force moment transfer is given by the point of intersection of the inclined line and the vertical line.

4.6.5 Introducing frictional force moment in the normal force equations

After introducing tangential forces into the normal force moment equations, we get the following equations:

$$(v_i^{n+} - v_i^{n-})m_i = \sum_k R_{ik}\hat{n}_{ij}\hat{n}_{ik} + \sum_k T_{ik}\hat{n}_{ij}\hat{t}_{ik}, \tag{85}$$

$$(v_j^{n+} - v_j^{n-})m_j = \sum_l R_{jl}\hat{n}_{ji}\hat{n}_{jl} + \sum_l T_{jl}\hat{n}_{ji}\hat{n}_{jl}. \tag{86}$$

Using $R_{ij} = -R_{ji}$ and isolating for R_{ij} we may write:

$$R_{ij} = m_{ij}^n \left(\frac{-\bar{v}_{ij}(1+\rho_n)}{\rho_n} \right) + K_{ij}, \tag{87}$$

where

$$K_{ij} = m_{ij}^n \left(-\frac{1}{m_i}\sum_{k\neq j} R_{ik}\hat{n_{ij}}\hat{n_{ik}} - \frac{1}{m_i}\sum_{k\neq j} T_{ik}\hat{n_{ij}}\hat{t_{ik}} + \frac{1}{m_j}\sum_{l\neq i} R_{jl}\hat{n_{ji}}\hat{n_{jl}} + \frac{1}{m_j}\sum_{l\neq i} T_{jl}\hat{n_{ji}}\hat{t_{jl}} - v_{ij}^{n-}(1+\rho_n) \right) \tag{88}$$

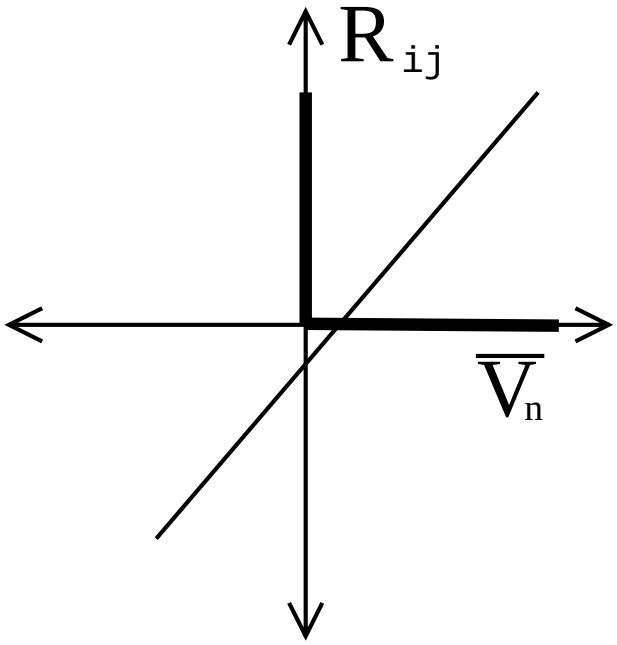

Figure 14: The Signorini graph is plotted together with the force moment transfer as a function of the formal velocity $\bar{v}_n$. The restitution equation(66) is only valid when $\bar{v}_n = 0$, and only in this case R will be larger than zero. If $\bar{v} \neq 0$, we have an open contact and $R = 0$. The inclined line represents the normal force moment during the collision as a function of the normalised velocity. Hence, the intersection point between the bold graph and the inclined line will give the normal force moment during the collision.

Again we see that if not the formal normal velocity is zero, the contact is inactive, because this implies that the restitutional relation fails. This gives us the same kind of Signorini graph as already shown is fig. 14.

4.7 The spin transfer

We also implemented a spin transfer, allowing a force moment to work on the two particles in contact during the collision. This pure spin transfer is useful when e.g. modelling porous packings. A Coulombian friction law is not enough to stop one bead from moving over another because it can simply roll. Now let us assume that one neighbour particle transmits an amount of spin ΔS to one of it's neighbours. Due to the geometry and adhesion there is an upper limit for ΔS, r_s. Next, the spin transfer is calculated in the following manner:

- 1. Calculate the spin transfer $\Delta S'$ necessary to stop the relative rotation.
- 2. Use the following condition:

$$\begin{cases} \Delta S' > r_s & \Rightarrow \quad \Delta S = r_s \\ \Delta S' \leq r_s & \Rightarrow \quad \Delta S = \Delta S'. \end{cases} \tag{89}$$

If the amount of spin transfer necessary to stop the relative rotation between two particles is larger than r_s, the relative rotation after the collision will not be zero, but only reduced.

4.8 The spin equations

The equations for the spin change of the particles i and j are:

$$I_i\omega_i^+ - I_i\omega_i^- = \sum_{k\neq j} T_{ik}r_i^2 + \Delta S \tag{90}$$

$$I_j\omega_j^+ - I_j\omega_j^- = \sum_{k\neq i} T_{jl}r_j^2 - \Delta S, \tag{91}$$

where ΔS is the transfer of spin from particle j to particle i. Next, we divide by the moments of inertia, and solve for ΔS given that $\omega_i^+ - \omega_j^+ = 0$:

$$\Delta S = \bar{m}^s(-\omega_i^- + \omega_j^- - \sum_k T_{ik}r_i^2 + \sum_k T_{jl}r_j^2,) \tag{92}$$

where

$$\frac{1}{\bar{m}^s} = \frac{1}{I_i} + \frac{1}{I_j}. \tag{93}$$

If we define the formal rotational velocity as

$$\bar{\omega}_{ij}^s = \omega_i^+ - \omega_j^+, \tag{94}$$

then we can represent the non-smooth condition on ΔS as the step-like function in Fig. 15.

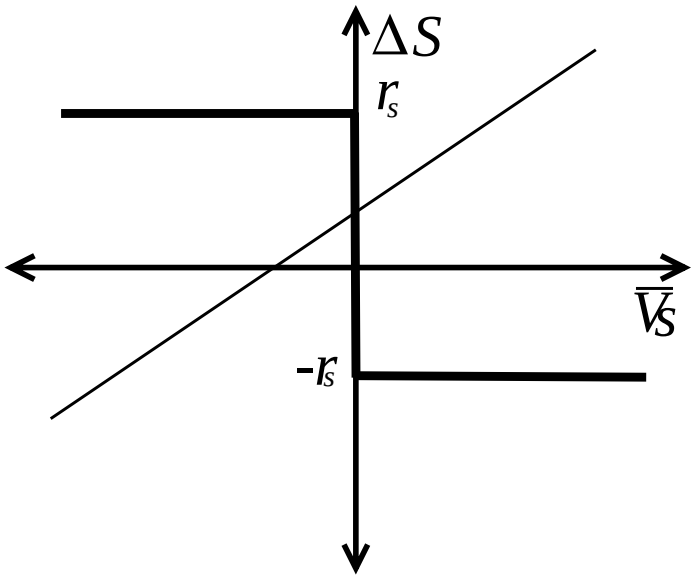

Figure 15: One plot is the non-smooth condition eq. (89) as a function of $\bar{v}_s$. The inclined line represents the spin transfer as a function of $\bar{v}_s$. The parameter r_s represents the limit of the spin transfer. The spin transfer during the collision is found in the crossing of the non-smooth spin condition function and the inclined line.

4.8.1 Numerical approach

Now there are enough equations to solve the system by setting up a matrix and inverting it. However, it is also possible to iterate towards the solution.

The equation for the solution of the normal force moment can be written:

$$R_{ij} = m^n_{ij}\bar{v}^n_{ij}. + K_{ij} \tag{95}$$

The first term on the right hand side is the force moment transfer in contact (ij), while the second term contains the indirect force moment transfer between the two particles. The solution for the tangential force moment can be written in the same manner:

$$T_{ij} = m^t_{ij}\bar{v}^t_{ij}. + L_{ij}, \tag{96}$$

where the first term contains the properties of the contact (ij), and the other term contains properties of all the other contacts. A similar equation is also written for the spin:

$$\Delta S_{ij} = m^s_{ij}\bar{v}^s_{ij}. + M_{ij}. \tag{97}$$

Then, by initially guessing the sets $(\{K\},\{L\},\{M\}) = (\{K_0\},\{L_0\},\{M_0\})$, one can find the first approximation of $(\{R\},\{T\},\{\Delta S\})$ by using the equations above and the non-smooth conditions connected to each equation. Then again, a new estimate $(\{K_1\},\{L_1\},\{M_1\})$ is found. For each iteration the contact network must be updated. If one normal force moment is found to be negative, the contact must be removed from the system. The tangential force moments, $\{T\}$, must be checked if they are inside the Coloumb limit or outside, and the equations in the iterator must adapt to the changes. Likewise, the normal forces and the spin transfers must be checked for their validity and the equations changed if necessary. By repeating the iterations, a solution is found.

4.8.2 The Non-Smoothness in Contact Dynamics

In the CD algorithm, the contact forces are subject to non-smooth conditions. This is in accordance with the formulation of the laws, the Coulomb friction law and the Signorini Condition. In Molecular Dynamics it is not possible to introduce non-smooth conditions as the algorithm is based on a integration of the parameters[2, 19, 20].

5 Stick-slip and Self-Organised Criticality

The second paper focuses on the stick-slip behaviour of a sheared granular column. This section contains a brief introduction to the topic.

The propagation of stress in granular media presents a complex problem which has been the subject of extensive study[56]-[58]. An applied external stress results in the

development of an internal structure, resisting the stress. The contact forces are not distributed uniformly[35]. The network of forces is believed to be the reason for jamming and fragility observed [59]-[60].

On characteristic of granular matters is a stick-slip behaviour when it slowly sheared [61, 62, 63]. The statistics of the stick-slip motion may reveal important properties of the force network. A large span in the stick and slip forces reflects a large span in the distribution of contact forces. It is also interesting to compare the statistics with other physical systems like the Gutenberg-Richter law for earth quake [64]. It is believed that simple systems can be used to describe complex processes [65]. In the second paper we investigate the stick-slip behaviour of particles in a two-dimensional column which is pushed at a constant velocity upwards, using the Contact Dynamics (CD) method. As a result, a very rich system is found.

In the headline of this section the Self-Organised Criticality is mentioned. Even though we can not claim that we have found evidence of SOC in the simulations, this field is so related that it should be commented. In [66] we can read that "Self-organised criticality is based upon the idea that complex behaviour can develop spontaneously in certain many-body systems whose dynamics vary abruptly. Researchers have observed characteristic general behaviour in systems as diverse as earthquakes, sand piles, and even biological evolution" In a famous paper Bak, Tang and Wiesenfield [67] claimed that complex systems which were driven by an external force could in some cases be characterised by quite general rules. General refers here to the aspect that the rules could be used to describe widely different systems. They are complex because the total system description is complex, and simple because different distributions can be described by the help of power laws. The term *Self-Organised* comes from the claim of Bak et al. [67] that complex systems turn into SOC states without tuning. The term *Criticality* comes from the claim that these systems behaved like equilibrium systems at the critical point.

In [66] it is claimed that there must be an evidence of power law both in time and in space before it is possible to speak about SOC. This must be so, because temporal fluctuations should reflect the spatial fluctuations. In our simulations, we have not been able to find more than one power law. This does not mean that no other power laws exist, but that they can be difficult to find due to the noise. One problem which occurred in the analyses of the stick-slip pattern was the presence of step-like functions, these functions have a very wide bandwidth, which disturbed the spectrum analysis.

6 Summary

One of the aims of this study was to test the Contact Dynamics method on different fields. We have shown how it can be used to produce more realistic structures of two-dimensional packings. Collective reorganisations can be significant, and could be the

topic for a separate study. Anyway this simulation work makes it possible for scientists in the field of packings to compare simple models with a more physical realistic model. In the other simulation work, we studied the steady-state flow of a granular column inside a narrow pipe. The finite stiffness of the pushing mechanism entailed a strongly irregular intermittent flow when the contacts were governed by a velocity weakening friction law. We found the following: 1) A transition to constant flow occurs for a driving velocity $v_t = (m/k)^{1/2}g$ involving no internal length and times scales; 2) The mean static driving force was correctly predicted by the Janssen model; 3) The distribution of force drops during slip events fell off as a power law over three decades with an exponent which did not seem to depend strongly on system parameters; 4) The slip events were preceded by creep motion leading most of time to an increase of the solid fraction, whereas slip events generally involved a dilation of the material. The origin of the broad distribution of event sizes remains an open question.

The third paper describe an experimental study: The apparent mass and the height of the packings have been measured for dynamic as well as static situations. For an upward motion the observations are consistent with a compactification front. The top did not start to move before this front reached the top. After the top started to move, the packing continued to compactify and the apparent mass increased monotonically until reaching a regime of stick-slip behaviour.

A creeping relaxation was observed in the static regime (regime 2) that may be explained by a combined ageing effect of the friction force, and a collective effect due to internal restructuring of the contact points.

For downward motion, we observed a de-compactification of the packing. The apparent mass decreased almost linearly before reaching a steady state. After the top had started to move for the downward motion, the height of the packing remained almost constant. This was not so for the upward motion so the process of translation up or down are not reversible.

Even for very small diameters, the apparent mass after directing the shear forces from the wall at the packing has an exponential decay. But the Janssen law does not fit satisfactory, and we argue for a two-parameter fit for small systems. The necessary condition for a exponential decay is shown to be rotational frustration and that the frictional forces are directed due to translation of the packing. The exponential decay is not observed for a column so narrow that each bead has only two neighbours. The two parameter Janssen law is observed to hold for the static case, which is the common setting. It also holds for upward movement and downward movement as well. For the narrow cylinders as was used in this experiment, it is not possible to fit the Janssen law's dependence on the diameter. The packing structure is the dominant factor for such small diameters.

References

[1] J.J. Moreau, Eur. J. Mech. A/Solids **13** (n° 4-suppl.), 93 (1994).

[2] M. Jean, in *Mechanics of Geometrical Interfaces*, edited by A.P.S. Selvaduri and M.J. Boulon (Elsevier, Amsterdam, 1995) p. 463.

[3] F. Radjai, Computer Physics Communications **121-122**, 294 (1999).

[4] L. Rothenburg and R. J. Bathurst, Géotechnique **39**, N° 4, 601-614 (1989).

[5] A. Gervois and D. Bideau, in *Disorder and Granular Media*, edited by D. Bideau and A. Hansen (North-Holland, Amseterdam, 1993) p. 1.

[6] J. Feder. Flow in porous media. Lecture notes, Physics Dept., University of Oslo, Norway, 1995

[7] P.Meakin and R.Jullien, J. Physique **46**, 1543 (1987).

[8] G. D. Scott, Packing of equal spheres, *Nature*, 188:908-909, 1960.

[9] *http://www.uis.edu/ trammell/MaterialsScience/Unit_Cells/*

[10] G.Y. Onoda and E.G. Liniger. Random loose packings of uniform spheres and the dilatancy onset. Phys Rev. Lett., 64:2727-2730, 1990.

[11] J.D. Bernal, Nature (London) **185** 68 (1960).

[12] A. Angell, J.H.R. Clarke, L.V. Woodcock, Adv. Chem. Phys. **48**, 397 (1981).

[13] R.A. Davis, H. Deresiewicz, Acta Mecanica **27** 69 (1977)

[14] D. Houi, Hydrodynamics of dispersed media Editors J.P.Hulin, A.M. Cazabat, E.Guyon, F.Carmona, Elsevier Science Publishers B.V (1990)

[15] A.B. Yu, J. Bridgewater, A. Burbidge, Powder Technology 92 185 (1997).

[16] R.Y. Yang, R.P. Zou, A.B. Yu, Phys. Rev. E **62** 3 (2000).

[17] P.K. Watson, H. Mizes A. Castellanos, A. Mizes, Powders and Grains 109 (1997).

[18] E.M. Tory, N.A. Cochrane, S.R. Waddell, Nature (London) **220** 1023 (1968).

[19] XJ. Schäfer, S. Dippel, and D.E. Wolf, J. Phys. I **6**, 5 (1996).

[20] F. Radjai, J.Schäfer, S.Dippel, and D. Wolf, J. Phys. I **7**, 1053 (1997).

[21] W.M. Visscher and M. Bolsterli, Nature (London) **239** 504 (1972).1

[22] E.M. Tory, B.H. Church, M.K. Tam, M. Ratner, Can. J. Chem. Eng. **51** 484 (1973).

[23] R. Jullien and P. Meakin, Europhys Lett. **6** 629 (1988).

[24] C.H. Bennet, J. Appl. Phys. **43** 2727 (1972).

[25] A.J. Matheson, J. Phys. C **7** 2569 (1974).

[26] Y. Koakawa, K. Ishizaki, Powder Technology **63** 241 (1990).

[27] J.L.Finney, Mater. Sci. Eng. **23** 199 (1976).

[28] W.S. Jodrey and E.M. Tory, Phys. Rev. A **32** 2347 (1985).

[29] A.S. Clarke and J.D. Wiley, Phys. Rev. B **35** 7350 (1987).

[30] G.T. Nolan, P.E. Kavanagh, Powder Technology **72** 149 (1992).

[31] G.C. Barker, A. Mehta, Phys.Rev. A **45** 3445 (1992).

[32] A.S. Clarke and H. Jonsson, Phys. Rev. E **47**, 3975 (1993).

[33] R. Jullien, P. Jund, D. Caprion, D.Quitmann, Phys.Rev. E **54** 6035 (1996).

[34] A. Yang, C.T. Miller and L.D. Turcoliver, Phys. Rev. E **53**, 1516 (1996).

[35] Liu, C. H., S. R. Nagel, D. A. Schecter, S. N. Coppersmith, S. Majumdar, O. Narayan, and T. A. Witten, 1995, Science **269**, 513.

[36] Dantu, P., 1957, Proc. 4th Int. Conf. Soil Mech. Found. Engng. **1**, 144

[37] J. P. Witmmer, M. E. Cates, and P. Claudin, *Stress propagation and arching in static sandpiles*, J. Phys. I **7** (1997)

[38] *The transmission of stress in an aggregate* S.F. Edwards, R.B.S. Oakeshott Physica D **38** (1-3): 88-92 (1989)

[39] *Model for force fluctuations in bead packs* S.N. Coppersmith, C.-h. Liu, S. Majumdar, O. Narayan, and T.A. Witten. Phys. Rev. E. **53**:4673-4685 (1996)

[40] *Granular matter: a tentative view* P. G. de Gennes Rev. Mod. Phys. **71** 2 (1999)

[41] *Force distributions in dense two-dimensional granular systems* F. Radjai, :M. Jean, J.J. Moreau, and S. Roux Phys. Rev. Let. **64** 2727-2730 (1990)

[42] H.M. Jaeger, and S.R. Nagel Rev. Mod. Phys. **68**, (1996)

[43] See e.g.: Chen Y.C., Ishibashi I. and Jenkins J.T., *Geotechnique* **38** (1988) 25, 33 and references therein.

[44] H.A. Janssen, Z.Ver. Dtsch. Ing. **39**, 1045 (1895).

[45] CV Schwab, IJ Ross, GM White, DG Colliver, Transactions of the ASAE **37**, 1613 (1994).

[46] SA Thompson, N Galili, RA Williams, Transactions of the ASAE **39**, 1093 (1996).

[47] J. Smid and J. Novosad. Pressure distribution under heaped bulk solids. *I. Chem. E Symposium Series*, 63:D3/V1-D3/V1/12,1981.

[48] Bouchaud J.-P., Cates M.E. and Claudin P., J. Phys. II France **5** (1995) 639.

[49] Evesque, P., and P. G. de Gennes, 1998, C. R. Acad. Sci. (PARIS), Ser. II, **326**, 761.

[50] *Surface flows of granular materials: A modified picture for thick avalanches* Boutreux, T. et al., 1998 Phys. Rev. E 58, 4692.

[51] Duffy A., and M. Mendlin, 1957, J. Appl. Mech. (ASME), **24**. 585.

[52] Savage, S. B., 1997a, Disorder and Granular Media (North-Holland, Amsterdam)

[53] Savage, S. B., 1997b, in Powders and Grains, edited by R. Behringer and Jenkins (Balkema, Rotterdam), p. 185.

[54] Goddard, J., 1998, in Physics of Granular Media, Proceedings of NATO Institute, edited by H. Herrmann, J. P. Hovi, and S. Luding (Kluwer Academic, Dordrecht).

[55] W.Goldsmith, *Impact: The Theory of Physical Behaviour fo Colliding Solids (London: Arnold, 1960)*

[56] J. Geng *et al.*, Phys. Rev. Lett. **87** 035506 (2001).

[57] G. Reydellet and E. Clement, Phys. Rev. Lett. **86** 3308 (2001).

[58] L. Vanel *et al.*, Phys. Rev. Lett. **84** 1439 (2000).

[59] M.E Cates, J.P. Wittmer, J.-P.Bouchaud, and P.Claudin, Phys. Rev. Lett. **81** 1841 (1998).

[60] M.E. Cates and J.P. Wittmer, Physica A **263**, 354 (1999).

[61] E. Kolb, T. Mazozi, E. Clment, and J. Duran, Eur. Phys. J. B **8**, 483 (1999)

[62] B. Miller, C. O'Hern, and R.P. Behringer, Phys. Rev. Lett. **77**, 3110 (1996).

[63] M. Lubert, A.de. Ryck, Phys. Rev. **63** (2001)

[64] B. Gutenberg and C. F. Richter, Ann. Geofis. **9**, 1-15 (1956).

[65] H.J.S. Feder and J.Feder, Phys. Rev. Lett. **66**, 2669 (1991).

[66] In Self-Organized Criticality by Henrik Jeldtoft Jensen, edited by P. Goddard, and J. Yeomans, Cambridge University Press, (1998).

[67] P. Bak, C. Tang, and K. Wiesenfeld, Phys. Rev. Let. **59**, 381 (1987)

[68] For recent contribution and discussion in this issue see: *Sands, powders and grains , An introduction to granulare materials*, edited by J. Duran, (Springer 1999),and reference herein.

[69] M. Jean, J.J. Moreau, in Contact Mechanics, edited by A.Curnier, Proceedings of the Contact Mechanics International Symposium, edited by A.Curnier 31-48 (Presses Universit Romandes, Lausanne 1992).

[70] M.P. Allen and D.J. Tildesley, *Computer simulation of liquids*, (Oxford Science Publications, New York, 1997).

[71] S. Luding in *Physics of Dry Granular Media* (NATO ASI Series) edited by H.J. Herrmann, J.-P. Hovi and S. Luding (Kluwer Academic Publishers, Dordrecht, 1998) p. 285.

[72] *Theory of powders Physica A* S.F. Edwards, R.B.S. Oakeshott **157** (3): 1080-1090 (1989)

[73] L. Vanel, E. Clement, Eur. Phys. J B **11** 525 (1999)

[74] T. Jotaki, R. Moriyama, J. Soc. Powder Technol. Jap **14**, 609 (1977).

[75] J.H Shaxby, J.C. Evans, Trans. Faraday Soc. **19**, 60 (1923).

[76] V. Frette, K. Christensen, A. Malthe-Sørensen, J. Feder, T. Jøssang, and P. Meakin. Avalanche dynamics in a pile of rice. *Nature*, 379:49-52, 1996.

Paper one

URN:NBN:no-3475

Dynamic rearrangements and packing regimes in randomly deposited two-dimensional granular beds

I. Bratberg*
Department of Telecommunications, Norwegian University of Science and Technology, N-7491 Trondheim, Norway

F. Radjai
LMGC, CNRS-Université Montpellier II, Place Eugne Bataillon, 34095 Montpellier cedex, France

A. Hansen
Department of Physics, Norwegian University of Science and Technology, N-7491 Trondheim, Norway
(Received 15 May 2002; published 19 September 2002)

We study the structural properties of two-dimensional granular packings prepared by random deposition from a source line. We consider a class of random ballistic deposition models based on single-particle relaxation rules controlled by a critical angle, and we show that these local rules can be formulated as rolling friction in the framework of dynamic methods for the simulation of granular materials. We find that a packing prepared by random deposition models is generically unstable, and undergoes dynamic rearrangements. As a result, the dynamic method leads systematically to a higher solid fraction than the geometrical model for the same critical angle. We characterize the structure of the packings generated by both methods in terms of solid fraction, contact connectivity, and anisotropy. Our analysis provides evidence for four packing regimes as a function of solid fraction, the mechanisms of packing growth being different in each regime.

DOI: 10.1103/PhysRevE.66.031303 PACS number(s): 83.80.Fg, 74.80.Bj, 81.05.Rm

I. INTRODUCTION

Random ballistic deposition (RBD) is a well-known method for layer-by-layer construction of random packings of hard particles such as granular beds and colloidal aggregates [1,2]. This method is based on a simple and intuitive procedure. The particles (mainly monodisperse spheres or disks) are allowed to fall sequentially along randomly positioned vertical lines over a horizontal substrate. Upon contact with the substrate or the first (already deposited) particle, the particle either sticks or is further moved to a more favorable position according to a relaxation (or restructuring) rule. The RBD method can be efficiently implemented in a computer code for generating very large two- and three-dimensional packings. Elaborate large-scale simulations based on this approach have been used to investigate the geometrical properties of random packings (packing regimes, distribution functions, growth, etc.) [3,4].

It is obvious that the random deposition of particles can also be simulated by means of dynamic methods, such as molecular dynamics [5,6] and contact dynamics [6–9], in the spirit of a real experiment where the grains are poured into a box. Such simulations require, however, substantially more computation time [10]. This difficulty has been inhibiting enough to discourage for a long time systematic investigation of deposited beds following dynamic methods. But, the situation is far better today due to the fast increase of available computer power and memory during the last decade. There is now a considerable scope for dynamic simulations that can be exploited in order to study a number of highly interesting issues in the field of random packings.

The objective of the present paper is to apply a contact dynamics algorithm to investigate randomly deposited granular beds in a two-dimensional (2D) geometry. The geometrical texture (coordination number, solid fraction, ...) of a granular bed depends on several physical parameters (particle properties, contact interactions, inertia of deposited particles) which can be tuned in a dynamic simulation in order to characterize the impact of each parameter on the texture. We propose here an approach that allows to bring out some interesting features of granular beds in comparison to RBD models. We consider a generalized RBD model in which the relaxation of the falling particle upon contact with the substrate is controlled by the direction of the contact normal θ (a single angle in 2D) [11]. Depending on whether θ is below or above a critical angle θ_c, the particle either simply sticks or is allowed to rotate until it reaches a local minimum position or forms a new contact below θ_c. Hereafter, we refer to this model as the critical angle (CA) model. The central feature of this model is that it allows to control the solid fraction ρ by varying the critical angle [11]. The approach we propose consists in performing dynamic simulations of random ballistic deposition *as closely as possible to the CA model*.

This requires that we transcribe the above geometrical relaxation rule into a contact law that is reduced to the geometrical rule for the random deposition process. We first show that this requirement is met if the particles interact through a *rolling friction* law (similar to the Coulomb sliding friction) in which a contact torque is mobilized to resist relative rotation of two particles. We implement this law within a contact dynamics (CD) algorithm. Then, we perform two series of simulations both with the CA model and the CD method. In the first series, we use the granular beds prepared

*Present address: Fysisk Institutt, Universitetet i Oslo, Postboks 1048 Blindern, N-0316 Oslo, Norway.

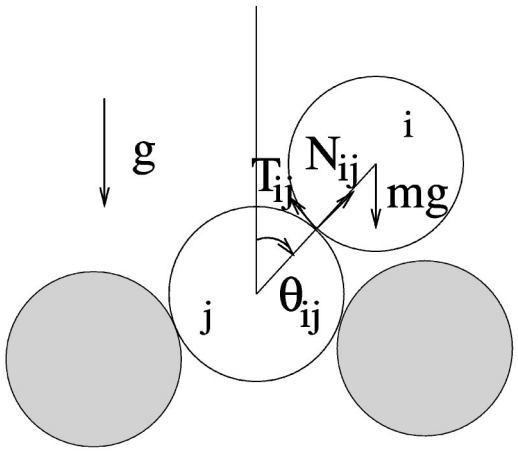

FIG. 1. Geometry of a contact formed by a falling particle *i* with a particle *j* from the substrate. The contact angle θ_{ij} is measured from the vertical.

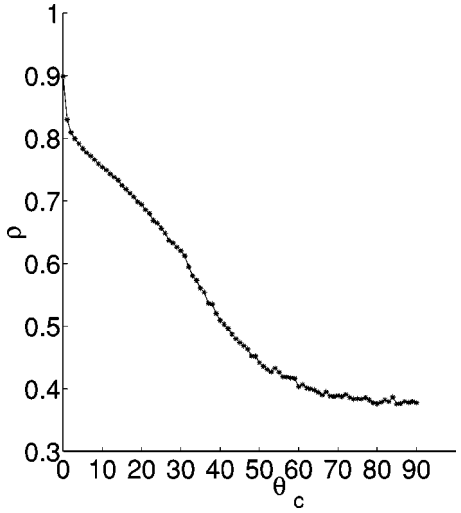

FIG. 2. Solid fraction ρ as a function of critical angle θ_c (in degrees) for the CA model.

according to the CA procedure as initial configuration for a CD simulation. We show that, although local stability (sticking due to rolling friction or, alternatively, particles supported by two underlying contacts) is fulfilled for each particle added to the bed, the latter still undergoes collective rearrangements leading to a higher solid fraction. This implies that a granular packing prepared by geometrical rules is globally unstable. We study the extent of dynamic rearrangements and the structural properties of the CA and CD packings as a function of the critical angle.

In a second series of simulations, we characterize the packings in terms of the average coordination number, structural anisotropy, and contact connectivity as a function of the solid fraction. We show that the trends are globally similar for the CD method and the CA model (the same packing regimes are observed). We distinguish several packing regimes where different mechanisms (screening, chaining, branching, piling, jamming, and ordering) are active and control the packing fraction.

II. NUMERICAL APPROACH

A. Critical-angle model

Figure 1 shows the geometry of a contact formed by a falling particle *i* with a particle *j* of the substrate. The two particle centers define a line inclined at an angle θ_{ij} to the vertical. For disks, θ_{ij} is also the direction of the contact normal $\boldsymbol{n}_{ij}$, unit vector directed from the center of particle *j* to the center of particle *i*. For brevity, we will refer to θ_{ij} as the ''contact direction.''

The CA model is defined as follows [11]. If $|\theta_{ij}|$ is below a critical angle θ_c, defined in the range between 0 (vertical direction) and $\pi/2$ (horizontal direction), the particle *i* simply freezes by sticking to particle *j*. On the other hand, if $|\theta_{ij}|$ exceeds θ_c, particle *i* is allowed to rotate around particle *j* until a second contact is formed with another particle *k* of the substrate. Then, there are three possible alternatives: (1) If $|\theta_{ik}|<\theta_c$, particle *i* freezes as in the first case; (2) if the new position of particle *i* is a local minimum position, again particle *i* freezes; (3) if neither of the two latter conditions is fulfilled, particle *i* is again allowed to rotate around particle *k* until a new contact is formed with another particle of the bed and the three alternatives are examined again with this new contact. This procedure is iterated until particle *i* is stabilized either by sticking or by reaching a local minimum position.

Two limits are of particular interest. When $\theta_c=90°$, all particles stick irreversibly to the substrate wherever they land. This limit corresponds to the random sequential adsorption model [12–15]. When $\theta_c=0°$, all particles relax and the model is reduced to the steepest descent model [1,16]. In Ref. [12], the solid fraction was found to be $\rho_{min}=0.3568\pm0.0001$ in the no-restructuring limit. The solid fraction for the steepest descent model is expected to come close to $\rho_{max}=0.906$ corresponding to a triangular packing. However, to achieve a structure with long-range ordering, the initial conditions are very important. In practice, the bottom line must initially be covered by an array of contiguous disks. Otherwise, simulations using the steepest descent algorithm have shown that the solid fraction will not exceed $\rho=0.82$, which is the characteristic density of 2D monodisperse random close packing where long-range order is broken by defects in the packing [12–17].

In the CA model, the solid fraction ρ of the granular bed is a function of the critical angle θ_c as shown in Fig. 2. In this figure, the solid fraction for each of the angles $\theta_c=0°,1°,2°,\ldots,90°$ is an average over 30 independent runs. The bottom line was covered by a layer of 32 contiguous particles and 1000 particles were deposited in each run. In order to avoid wall effects, periodic boundary conditions were implemented in the horizontal direction. Let us note that CA simulations are possible at much larger scales. Nevertheless, we restrict here the size and the number of CA simulations to those reasonably accessible to dynamic simulations since the results will be compared between these two methods below. Figure 2 shows that the solid fraction decreases monotonously from ρ_{max} to ρ_{min} as θ_c is increased from 0 to 90°. One can distinguish several regimes on this

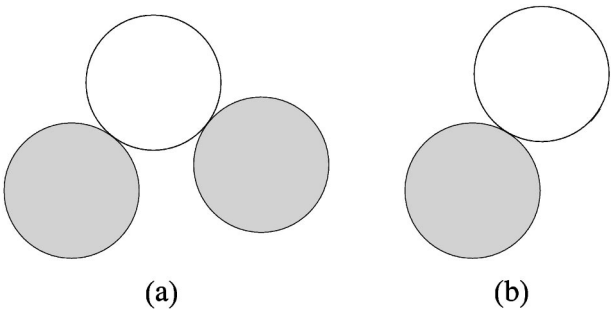

FIG. 3. The two local stability conditions in the CA model: (a) local minimum position, (b) sticking.

curve, which will be discussed below in connection with dynamic simulations.

The CA model is a geometrical model that meets the no-overlap condition between hard particles but involves a number of physical approximations about the stability of the packing and its growth. By nature, this model neglects inertia effects. The substrate is frozen and the relaxation step involves only the deposited particle. Moreover, the two stability criteria (local minimum position and sticking condition) for the deposited particle have a *local* nature. In other words, the model assumes that the whole packing remains in static equilibrium as long as all particles are sequentially stabilized by either of these conditions.

In order to examine the validity of these assumptions, the approach followed in this paper is to perform dynamic simulations as closely as possible to the CA model and to compare the resulting packings. This implies that the particles should be released sequentially and they should hit the granular bed with negligibly small inertia. Moreover, upon contact with the substrate, the falling particle should dynamically stick or roll down depending on the value of the contact angle with respect to the critical angle, until one of the two stability conditions is fulfilled. There is no difficulty in tuning the inertia in a dynamic simulation. But, we need to define a dynamic version of the relaxation rule.

B. Rolling friction

The dynamic content of stability due to a local minimum position is clear. The weight of a particle can obviously be balanced by the reaction forces exerted by two underlying particles; see Fig. 3(a). But the sticking condition requires both a contact force $\boldsymbol{F}_{ij}$ and a ''contact torque'' M_{ij} so as to counterbalance, respectively, the weight $m_i g$ of the deposited particle and its moment with respect to the contact point. Figure 3(b) illustrates this condition. The balance equations are

$$\boldsymbol{F}_{ij}+m_i\boldsymbol{g}=0, \tag{1}$$

$$m_i g r_i \sin\theta + M_{ij}=0, \tag{2}$$

where r_i is the particle radius and $\boldsymbol{g}$ is the gravity.

Let N_{ij} and T_{ij} be the components of the reaction force $\boldsymbol{F}_{ij}$ along and perpendicular to the contact normal $\boldsymbol{n}_{ij}$. From Eq. (2) one gets

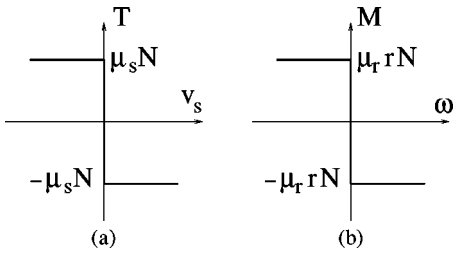

FIG. 4. The graphs representing (a) sliding friction law and (b) rolling friction law; see text.

$$N_{ij}=m_i g\cos\theta, \tag{3}$$

$$T_{ij}=m_i g\sin\theta, \tag{4}$$

$$M_{ij}=r_i N_{ij}\tan\theta. \tag{5}$$

The normal force N_{ij} is positive (as it should) as long as $-\pi/2<\theta<\pi/2$ (the angles are measured from the vertical). On the other hand, the relative sliding is inhibited if $|T_{ij}|/N_{ij}<\mu_s$, where μ_s is the coefficient of (sliding) friction (or equivalently, $\theta<\theta_s$, where $\theta_s=\tan^{-1}\mu_s$ is the angle of friction).

Now, if we require that particle i rolls only if $\theta\geqslant\theta_r$, then from Eq. (5) we arrive at the following no-rolling condition:

$$\frac{|M_{ij}|}{r_i N_{ij}}<\tan\theta_r=\mu_r, \tag{6}$$

where μ_r is a coefficient of *rolling friction*. Let us further assume that M_{ij} remains equal to its threshold value $\pm\mu_r r_i N_{ij}$ when rolling occurs. This condition is similar to the sliding condition $T_{ij}=\pm\mu_s N_{ij}$.

The rolling friction law, as defined here, and the more familiar Coulomb (sliding) friction law are shown in Fig. 4 in the form of graphs [8,18]. The rolling friction law relates the relative rotation velocity $\omega_{ij}=\omega_i-\omega_j$ of the two particles to the contact torque M_{ij}, whereas the sliding friction law relates the sliding velocity v_{ij}^s to the tangential force T_{ij}. In fact, although for the sake of clarity we derived the condition (6) by considering the particular case of a deposited particle touching a particle of the bed, the application of rolling friction to a contact between two arbitrary particles in a packing is rather straightforward when formulated in the form of the graphs shown in Fig. 4. The torque transmitted through a contact to a particle in static equilibrium, for example, is the torque necessary to balance the sum of all force moments and other contact torques acting on the particle in the same way as the mobilized torque M in Eq. (6) counterbalances the moment $rmg\sin\theta$ of the particle weight.

The prescription of rolling friction in a dynamic method follows the same steps as the sliding friction. The relation between the contact torque and the relative rotation velocity [Fig. 4(a)] cannot be represented as a monovalued function. Hence, in the framework of the molecular dynamics method, based on explicit integration of the equations of motion, this friction law has to be replaced by an approximate *function* [8,10,19]. This ''regularization'' of the friction law is not

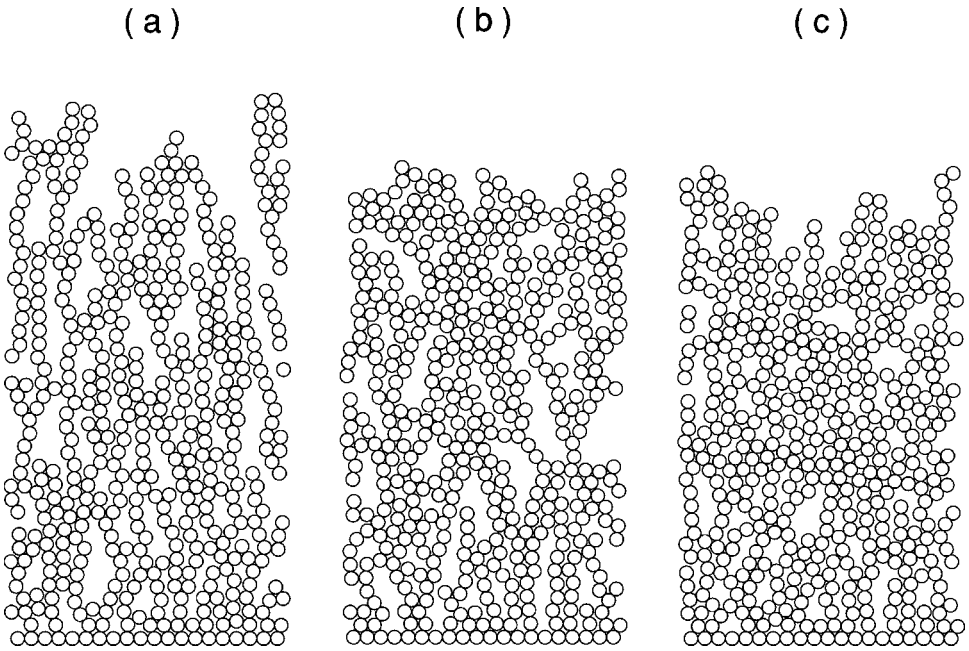

FIG. 5. (a) An example of a CA packing. (b) The static packing obtained by the CD method starting with the CA packing in (a) as initial condition, (c) CD packing obtained by using the same sequence of falling particles as in (a).

necessary within the contact dynamics method that was employed for the present investigation [7–9].

Using either of these dynamic methods, the sticking condition can be achieved if μ_s is set to infinity (no sliding for no contact direction) and the angle of rolling friction θ_r is interpreted as the critical angle θ_c. This was implemented in our contact dynamics simulations. Alternatively, one may set μ_r to infinity (no rolling for no contact direction) using the angle of sliding friction θ_s as the critical angle. It is also possible to use a combination of these two conditions. These conditions are not equivalent, but we will not discuss the differences in this paper. In all cases, the condition of sticking upon collision requires also a zero coefficient of restitution.

To summarize, the following conditions allow to perform a dynamic simulation of random particle deposition in close analogy with the CA model: (1) $\theta_r = \theta_c$, (2) no sliding ($\theta_s = 90°$), (3) weak inertia, (4) zero coefficient of restitution. The important difference is that, while in the CA model all degrees of freedom in the substrate are kinematically frozen, in our dynamic simulations only contact sliding is frozen by setting $\theta_s = 90°$. All other degrees of freedom are active and the rolling friction governs all contacts: the contact between the deposited particle and the bed, as well as all contacts in the bed. Since the particles are not frozen in the granular bed, sequential particle deposition may thus lead to rearrangements in the granular bed.

C. Simulation parameters

The CD simulations involve a number of parameters that should be adjusted so as to minimize inertia effects without losing numerical efficiency. The largest inertia effects are produced by the largest head-on velocity v_{max} between colliding particles. Let Δt be the time step. The contact force due to inertia produced by a collision is $mv_{max}/\Delta t$. This force should be compared to the weight mg of one particle. Hence, the dimensionless parameter characterizing the ratio of inertia to weights is

$$\alpha = \frac{v_{max}}{g\Delta t}. \tag{7}$$

The influence of α on the solid fraction and restructuring is an interesting subject in itself, but it will not be investigated in this paper. As emphasized previously, the focus here is put on those effects (equilibrium states, rearrangements) that arise from the *geometrical configuration*. Hence, we should use a low value of α. However, lower values of α mean slower simulations. Hopefully, the framework of the CD method allows for large time steps Δt up to the limitations related to the procedure of contact detection. On the other hand, the value of v_{max} can be imposed for the falling particles, but further relaxation inside the packing may produce large impact velocities. In particular, at low solid fractions, where large voids exist in the bed, the free fall of a particle over distances compared to the system height $H \simeq 60r$ can give rise to impact forces far larger than the weight of a column of particles of the same height.

In order to avoid such strong uncontrolled inertia, we implemented a ''velocity barrier'' trick that limits the particle velocities to $v_{max} = 0–3\ \mathrm{ms}^{-1}$. With this choice, we can use a time step as large as $\Delta t = 0.003$ s. Then, setting $g = 100\ \mathrm{ms}^{-2}$, we get $\alpha = 1$. This means that the largest impact force is just equal to the weight of a single particle. This choice is both reasonable and compatible with numerical efficiency.

III. DYNAMIC REARRANGEMENTS

A. Stability of CA packings

How stable are the granular beds prepared by means of the CA model? We have seen that the CD method, equipped

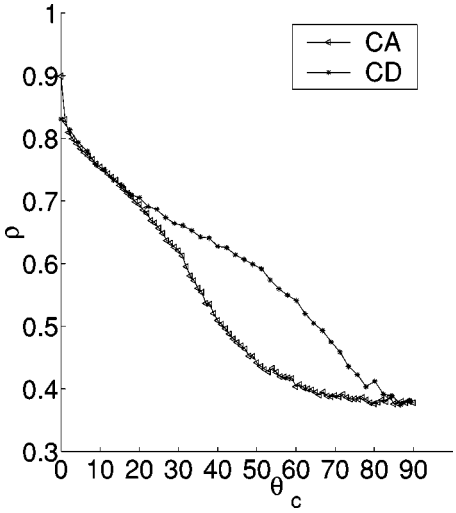

FIG. 6. Solid fraction as a function of critical angle (in degrees) for the CD and CA models.

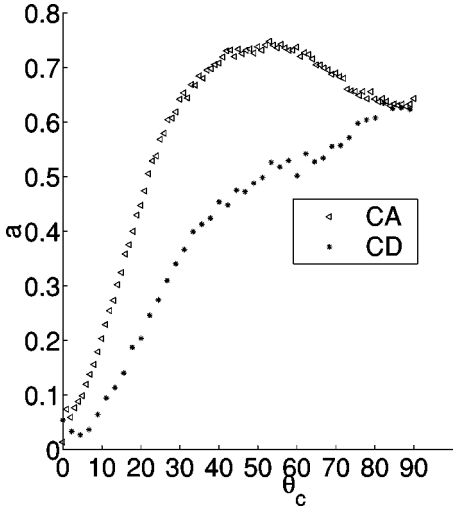

FIG. 8. Anisotropies a as a function of critical angle (in degrees).

with rolling friction together with suitable values of the parameters reducing inertia effects, meets the *single-particle* stability criteria of the CA model in the course of deposition, namely (1) the sticking condition as a function of the rolling friction angle θ_r (identified with the critical angle θ_c) and (2) the local minimum position where the weight of a particle is balanced by the reaction forces at the two underlying contacts. Now, if we start a CD simulation using a packing constructed according to the CA model as the initial configuration, then one of the two following alternatives may occur. If the single-particle stability criteria used in the course of deposition provide a sufficient condition for the *global* stability of the packing when the deposition is over, then the packing will remain in static equilibrium and the calculated forces will exactly balance all particles. Otherwise, the packing will be unstable and the CD simulations allow to calculate the particle rearrangements until a relaxed stable configuration is obtained.

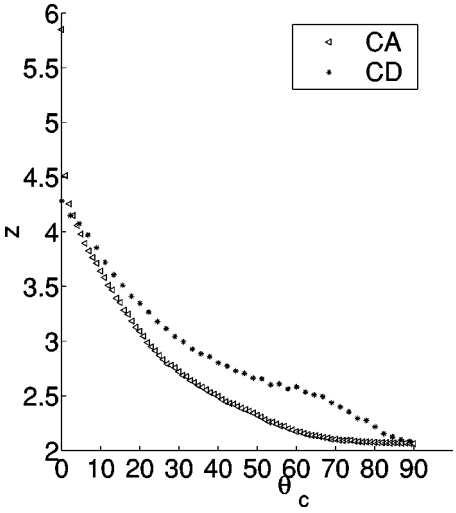

FIG. 7. Coordination numbers z as a function of critical angle (in degrees).

Our simulation data confirm rather the second alternative for nearly all values of the critical angle. One example is shown in Figs. 5(a) and 5(b) for a packing of 500 particles with $\theta_c = 40°$. The rearrangements occur in the whole bed, but they are much more hindered in the bulk than in the vicinity of the free surface. For this reason, the displacements appear mostly in the uppermost layers. The relaxed configuration has a larger packing fraction. The solid fraction is still larger when the CD simulation is performed by random deposition of the same sequence of particles (as in the CA simulation) for the same value of θ_c (and the same boundary conditions), instead of using the CA configuration as the initial condition. The resulting packing is shown in Fig. 5(c). In this latter case, the hindering effect related to the bulk density, which was active in the case [Fig. 5(b)], disappears since the CD rearrangements occur naturally in the course of deposition for each deposited particle. This means that the degree of instability of the CA packing shown in Fig. 5(a) is more keenly reflected in the increase $\Delta\rho$ of the solid fraction from Figs. 5(a) to 5(c) than from Figs. 5(a) to 5(b).

Figure 6 displays the solid fraction ρ as a function of θ_c

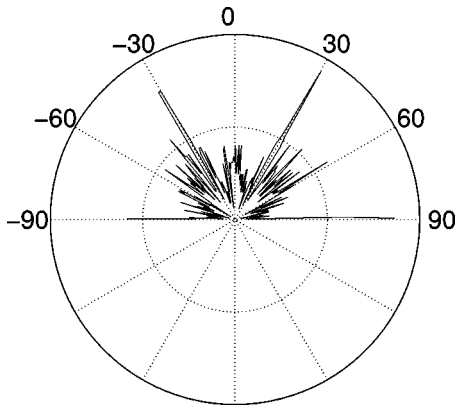

FIG. 9. Polar diagram of the distribution $p(\theta)$ of contact angles in a CD packing with $\theta_c = 0$. The zero angle refers to the vertical direction. The angles are in degrees.

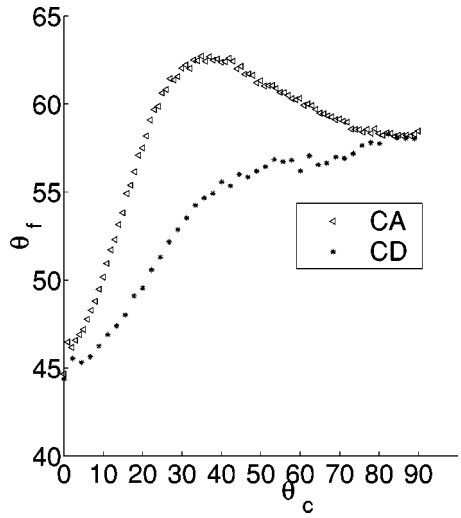

FIG. 10. The major principal directions θ_f of the fabric tensor as a function of critical angle. The angles are in degrees.

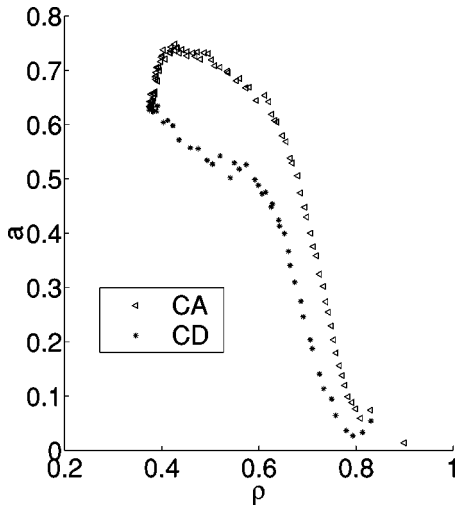

FIG. 12. Anisotropies a as a function of solid fraction.

for packings prepared by CD sequential random deposition. The solid fraction for each value of θ_c is an average over 10 independent CD runs. The CD simulations were performed for 40 different angles. The curve of ρ as a function of θ_c corresponds thus to 410 CD simulations of 1000 particles. Figure 6 shows that, as expected, the solid fraction is everywhere larger for the CD method than for the CA model, except at $\theta_c=0$ where a dynamic method requires an exceptionally high precision to reach a perfect triangular packing. Indeed, in this limit, tiny fluctuations in particle positions around a particle due to numerical overlaps are exponentially amplified in space as a result of long-range order [20]. Disregarding this pathological limit, the difference $\Delta\rho$ is negligibly small for $\theta_c<20°$ and $\theta_c>80°$. The largest variation $\Delta\rho$ of the solid fraction, representing the largest dynamic rearrangements in the packing, occurs at $\theta_c\simeq 50°$, where ρ increases from 0.45 for the CA packing to 0.6 for the CD packing.

B. Influence on the packing structure

The coordination number z (average number of contact particles around a particle), shown in Fig. 7 as a function of θ_c, follows the same trends as the solid fraction. It is systematically larger in a CD packing than in the corresponding CA packing (for the same value of θ_c) except in the $\theta_c=0$ limit. A coordination number close to 2 reflects the predominance of particle ''chains'' in a highly porous packing. The coordination number increases from 2 to 3 due to ''branching,'' and from 3 to 4 due to a growing interplay of chains. The increase of z beyond 4 requires long-range ordering [21]. This transition occurs only in the CA packing where the numerical precision is less stringent than in dynamic simulations.

Due to dynamic rearrangements in CD random deposition, the CA and CD packings show also very different aspects as to the directional order of the contact network. The nonuniform distribution of contact directions can be charac-

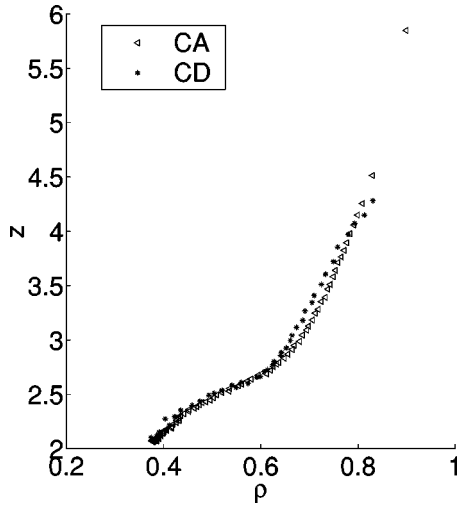

FIG. 11. Coordination numbers as a function of solid fraction ρ.

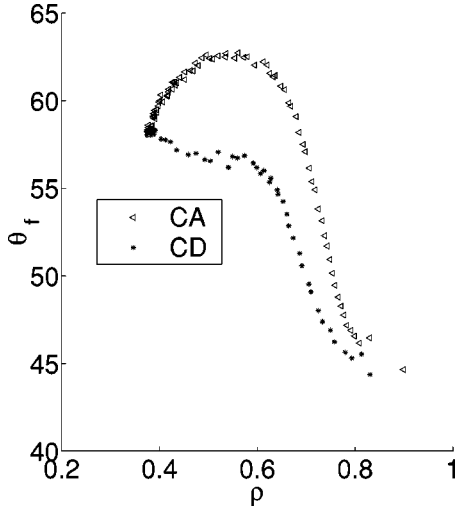

FIG. 13. The major principal directions θ_f (in degrees) of the fabric tensor as a function of solid fraction.

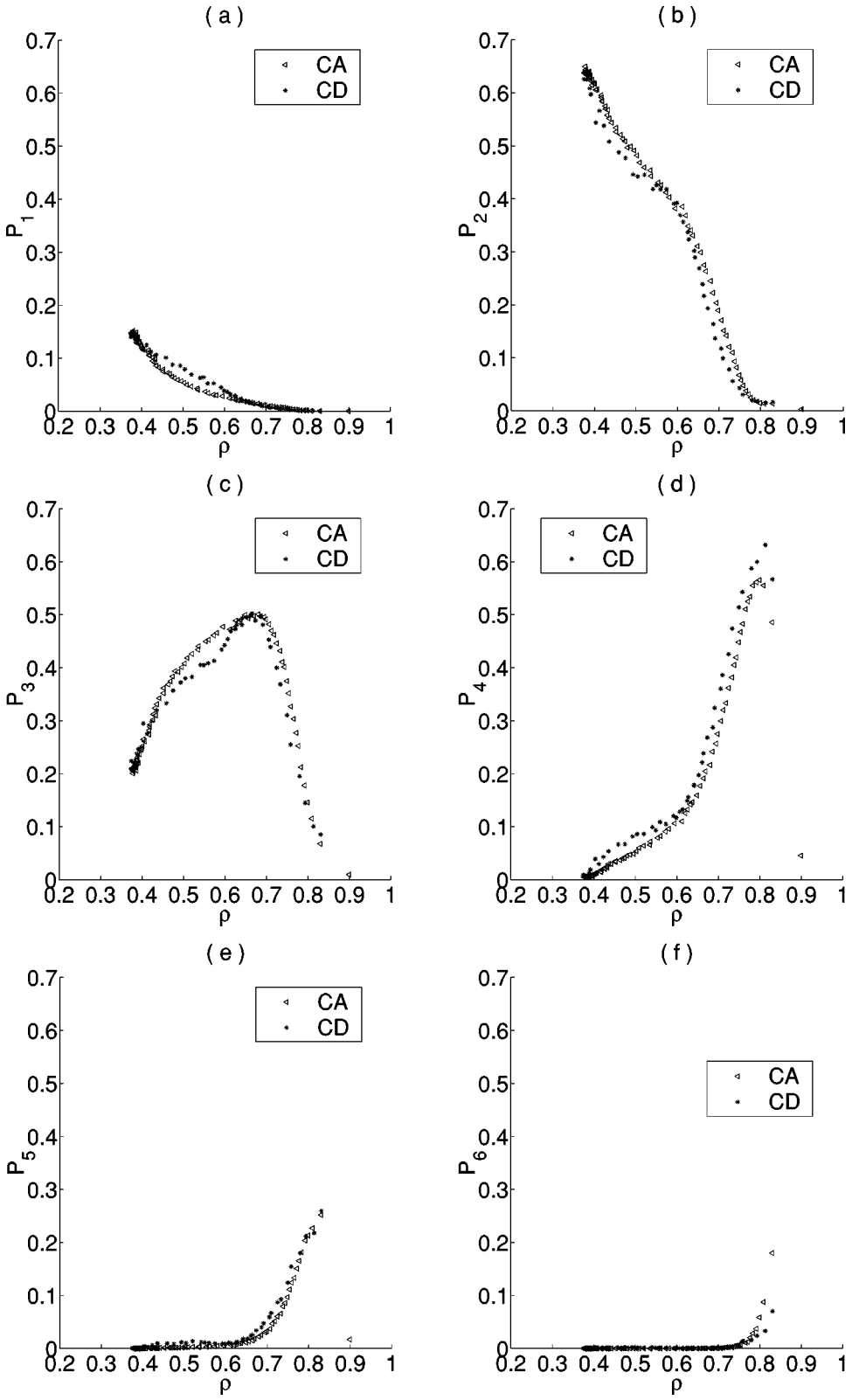

FIG. 14. The connectivity numbers $P_1, \ldots, P_6$ as a function of solid fraction.

terized by means of the fabric tensor $\boldsymbol{\phi}$ defined from contact normals $\boldsymbol{n}^k=(\sin\theta^k,\cos\theta^k)$ by [22,23]

$$\phi_{\alpha\beta}=\frac{1}{N_c}\sum_{k=1}^{N_c} n_\alpha^k n_\beta^k, \tag{8}$$

where N_c is the total number of contacts, and n_α^k (respectively n_β^k) is the α (respectively β) component of the contact normal k. When the probability distribution function $p(\theta)$ of contact directions is known, the fabric tensor can be calculated from the integral

$$\phi_{\alpha\beta} = \int_{-\pi/2}^{\pi/2} n_\alpha n_\beta p(\theta)\ d\theta. \tag{9}$$

By construction, we have $\phi_1 + \phi_2 = \mathrm{tr}(\boldsymbol{\phi}) = 1$, where ϕ_1 and ϕ_2 are the eigenvalues. The mean contact direction in the packing is given by the major principal direction θ_f of $\boldsymbol{\phi}$. The structural anisotropy of the packing is represented by $a = 2(\phi_1 - \phi_2)$. The factor 2 is introduced in order to identify this value of a with that appearing naturally in a sinusoidal distribution $p(\theta) = (1/\pi)\{1 + a\cos 2(\theta - \theta_f)\}$ [24].

Figure 8 shows the anisotropy of our granular beds as a function of θ_c. We see that the anisotropy of CD packings is systematically below that of CA packings. This is mainly because collective rearrangements tend to destroy columnar structures in a CD packing. In both cases, the anisotropy comes very close to zero for $\theta_c = 0$. This effect is mainly related to the presence of a great number of particles with five and six contacts. In fact, using Eq. (8), it can be shown that the anisotropy for the set of six contacts around a particle is zero, and for a set of five contacts around a particle cannot exceed a threshold imposed by steric exclusions.

The largest anisotropy in the CD packings is reached for $\theta_c = 90°$, whereas the anisotropy of the CA packing passes through a maximum at $\theta_c \simeq 50°$. The anisotropy can be estimated analytically at $\theta_c = 90°$, where the packing growth is governed by sticking. Since the particles are released at random horizontal positions, the probability that a particle sticks at a contact angle θ (with respect to the vertical) is $p(\theta) = \frac{1}{2}\cos\theta$. Note that the latter is a normalized probability density function over the range $[-\pi/2, \pi/2]$. Using Eq. (9) with this expression for $p(\theta)$, we find $a(\theta_c = 90°) = 2/3$, which is consistent with both CD and CA results at $\theta_c = 90°$ shown in Fig. 8.

Since $p(\theta)$ is an even function of θ $(p(\theta) = p(-\theta))$, the major principal direction of the fabric tensor is vertical $(\theta_f = 0)$. However, this is only a consequence of symmetry and it does not imply that the distribution $p(\theta)$ is peaked on $\theta = 0$. In fact, within each of the half intervals $[-\pi/2, 0]$ and $[0, \pi/2]$, the contacts have preferred directions. This can be seen in one example of $p(\theta)$ for $\theta_c = 0$ shown in Fig. 9. We observe a local maximum at $\theta = 0$, but there are local maxima also in each of the half intervals. In order to extract the useful information about the direction of contacts, one can calculate the fabric tensor $\boldsymbol{\phi}$ by restricting the definition to one of the above two half intervals.

The major principal direction θ_f for the interval $[0, \pi/2]$ as a function of θ_c is displayed in Fig. 10. At $\theta_c = 0$ and $\theta_c = 90°$ both methods give the same direction, but everywhere else the contacts are more biased to the horizontal direction in CD simulations compared to CA simulations. This is an indication that the collective rearrangements reorganize contact directions. As for the anisotropy, the value of θ_f can be calculated analytically in the limit $\theta_c = 90°$ over the interval $[0, \pi/2]$ from the fabric tensor. The distribution function normalized over this interval is given by $p(\theta) = \cos\theta$ and the integral in Eq. (9) is calculated over the same interval. We find $\theta_f(\theta_c = 90) \simeq 32°$, in agreement with the simulation result shown in Fig. 10.

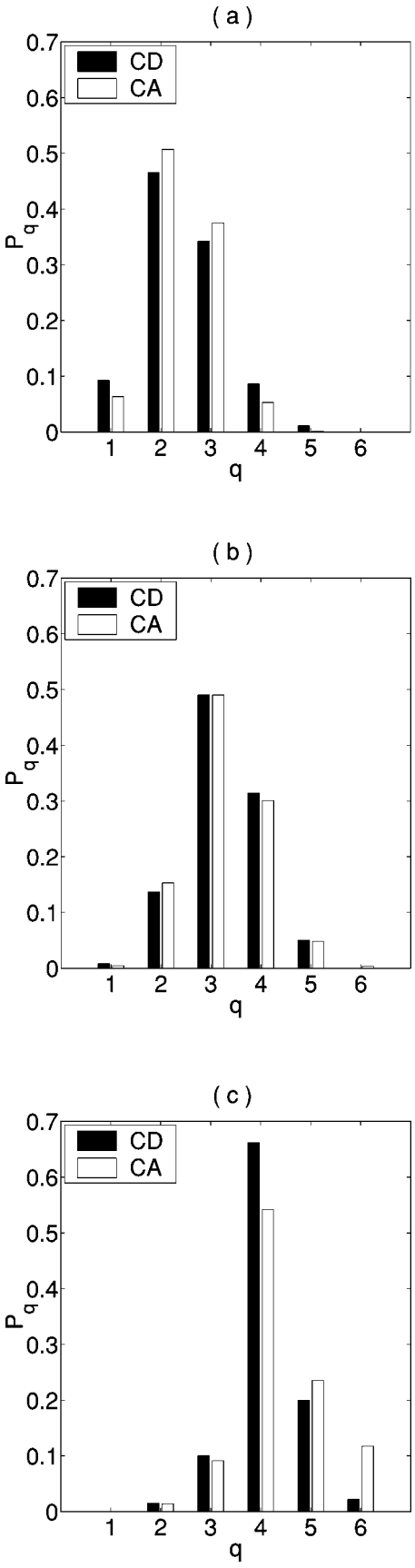

FIG. 15. The connectivity diagram of CA and CD packings at three different values of solid fraction: (a) $\rho = 0.5$, (b) $\rho = 0.7$, and (c) $\rho = 0.8$.

The existence of a local minimum in the evolution of θ_f for the CA model at $\theta_c \simeq 30°$ or the changing of behavior in the CD curve at the same point can be understood as a consequence of competition between sticking and rolling. As θ_c is increased from zero, an increasing number of particles stick to the substrate at an angle in the interval $[0,\theta_c]$. These include both the ones sticking to the bed upon the first collision (whose number increases as $\int_0^{\theta_c} \cos\theta\, d\theta = \sin\theta_c$) and a number of the relaxed particles. On average, this subset of contacts tends to decrease θ_f as long as θ_c is not too large. This explains the decrease of θ_f from 45° at $\theta_c = 0$ to $\simeq 28°$ at $\theta_c \simeq 30°$. But, the inclination of the contacts to the vertical increases at the same time following the increase of θ_c. This trend dominates clearly the evolution of θ_f beyond $\theta_c = 30°$.

IV. PACKING REGIMES

The results presented in the preceding section show that, for a given value of the critical angle θ_c, the solid fraction and the structure of the packing differ considerably from the CA model to the CD approach (excepted in the two limits of very loose and very dense packings). We attributed these differences to dynamic restructuring in CD packings as the particles are added to the substrate. However, in this section, we will show that the structure of a CA packing is quite similar to that of a CD packing if they are compared at the same solid fraction ρ (and thus, for different critical angles). This means that the structural properties of CA packings are quite realistic (close to CD packings) when they are considered as a function of the solid fraction rather than the critical angle.

A. Fabric

Figure 11 shows the coordination number z as a function of solid fraction ρ for CA and CD packings. In both cases, z increases with ρ. The two curves almost collapse for $\rho < 0.6$. For $0.6 < \rho < 0.8$, the CD packings show only a slightly larger coordination number than the CA packings. For $0.8 < \rho$, the CD packings show a slightly lower coordination number than the CA packings. The solid fraction $\rho = 0.8$ corresponds to $z \simeq 4$ in both methods.

The anisotropy a of the packings as a function of ρ is displayed in Fig. 12. The anisotropy decreases as a function of ρ for both methods except in the loosest CA packings where it increases a bit with ρ and passes through a peak before decreasing. The relatively low rate of decrease in the range $\rho < 0.6$ suggests that sticking is the dominant mechanism of growth in this regime, whereas rolling (or relaxation) is far more efficient in the subsequent range.

Figure 13 shows the major principal direction θ_f of the fabric tensor restricted to the interval $[0,\pi/2]$ (as defined in the preceding section) as a function of ρ. In CD packings, the direction θ_f, representing the average direction of contact normals in the interval $[0,\pi/2]$, increases quite slowly for $\rho < 0.6$ and much faster beyond 0.6. In CA packings, the anisotropy decreases for $\rho < 0.6$, passes through a minimum at $\rho \simeq 0.6$ and increases in the subsequent range. However, let us remark that, as for the anisotropy, the difference in the value of θ_f between the two methods as a function of ρ is quite small as compared to the differences as a function of the critical angle (see Fig. 10).

B. Connectivity

The coordination number z is an average over all particles in a packing. But, the number of contact neighbors q varies in a packing from particle to particle. In a monodisperse pile, q can vary from 1 to 6. This ''connectivity disorder'' characterizes the disposition of the particles as ''nodes'' of the contact network. The connectivity of a packing is given by the fraction P_q of particles having q contact neighbors. P_1 corresponds to the ''dead ends'' of particle chains. The larger P_1, the stronger is the ''screening'' (the dead ends did not grow because they were screened by faster growing structures). P_2 and P_3 are related to chaining and branching, respectively. P_4 corresponds to ''piling,'' i.e., a natural situation where a particle is supported by two underlying particles and supports two others. P_5 and P_6 define ''jammed'' and ordered configurations.

Figure 14 shows the connectivity numbers P_q as a function of solid fraction for q varying from 1 to 6. The trends are globally similar in CA and CD packings and the differences for the two methods are quite small. All connectivity numbers vary monotonously with solid fraction except P_3 that first increases to reach a maximum at $\rho \simeq 0.7$ and decreases rapidly afterwards. In the range $\rho < 0.6$, P_3 and P_4 increase at the expense of P_1 and P_2 which decrease. P_5 and P_6 begin to increase significantly only at $\rho \simeq 0.7$ and $\rho \simeq 0.8$, respectively.

The connectivity diagram P_q is shown for three different solid fractions in Fig. 15. The largest connectivity number is 2 for $\rho < 0.6$, 3 for $0.6 < \rho < 0.7$, and 4 for $0.7 < \rho$. Interestingly, the screening effect is more important in CD simulations (the CD curve for P_1 stands above the corresponding CA curve). Chaining (P_2), branching (P_3), and ordering (P_6) are slightly less important in CD simulations, while piling (P_4) and jamming (P_5) are enhanced.

The above data show that the morphology of a CA packing is very close to that of a CD packing at the same solid fraction. Both methods suggest four packing regimes characterized by the properties of the packing structure as a function of solid fraction:

(a) $\rho < 0.6$: This regime corresponds to loose random packings characterized by chaining (i.e., P_2 is the largest connectivity number), branching (P_3 increases as a function of ρ and becomes dominant at $\rho = 0.6$), and screening (P_1 is large).

(b) $0.6 < \rho < 0.7$: This is the regime of moderate random packings characterized by the largest value of P_3 (branching) at the expense of chaining (P_2) that decreases rapidly as a function of ρ.

(c) $0.7 < \rho < 0.8$: This regime corresponds to dense close packings where piling is the main mechanism of growth and P_4 is larger than other connectivity numbers.

(d) $0.8 < \rho$: This is the well-known dense ordered packing regime [18] characterized by $z > 4$.

The transition densities (0.6, 0.7, and 0.8) appearing in this classification are approximate values. A more refined evaluation of these specific densities requires a considerably more computation time and a deeper insight into the mechanisms at play during the packing growth.

V. CONCLUSION

We investigated the structure of a class of randomly deposited granular packings whose density is controlled by a geometrical parameter, referred to as the critical angle. We used both a random ballistic deposition model with simple relaxation rules (the CA model), and a contact dynamics algorithm (the CD method) that incorporates those relaxation rules through a rolling friction law. The CD approach naturally leads to stable packings following dynamic rearrangements while in the CA model the packing is kinematically frozen after each single-particle relaxation.

The following results were shown by means of extensive simulations:

(1) The packings prepared according to the CA model are generically unstable. When fed into the CD algorithm as initial configuration, the CA packings undergo dynamic rearrangements. As a consequence, the solid fraction is larger in CD packings than in CA packings for the same critical angle (implemented as the angle of rolling friction in the framework of the contact dynamics method).

(2) The structural properties (anisotropy, connectivity) are quite comparable in CA and CD packings for the same solid fraction, even though significant differences were observed in packing anisotropies.

(3) Both methods reveal four packing regimes as a function of solid fraction, the prevailing mechanism of growth being different in each regime.

An important outcome of this work is to show that the dynamic rearrangements are quite weak in the very loose and very dense limits where the structural properties are nearly the same. This means that the random sequential adsorption model (irreversible sticking without relaxation) leading to very loose packings, and the steepest descent model (no sticking) leading to very dense packings, can be used with confidence in these two limits.

The CD simulations reported in this work were meant to keep as close as possible to the CA model in order to perform comparable calculations with both methods. There is much more to be learned about the structure of particle packs generated by the CD method (or equivalently, molecular dynamics method). The influence of inertia and polydispersity on the observed packing regimes is currently under investigation. The shear resistance of deposited beds (e.g., in a biaxial compression) as a function of solid fraction is another important issue that we would like to address in near future.

ACKNOWLEDGMENTS

We thank Knut Jørgen Måløy, Anders Malthe Sørensen, Espen Gjettestuen, and Lothar Brendel for fruitful discussions. This work had its financial support by the Research Council of Norway (NFR) through a Strategical University Program. We are also grateful to the CNRS and NFR for support through the Franco-Norwegian PICS program, Grant No. 753.

[1] R. Jullien, P. Meakin, and A. Pavlovitch, in *Disorder and Granular Media*, edited by D. Bideau and A. Hansen (North-Holland, Amseterdam, 1993), p. 103.
[2] D. Houi, in *Hydrodynamics of Dispersed Media*, edited by J.P. Hulin, A.M. Cazabat, E. Guyon, and F. Carmona (Elsevier Science B. V., Amsterdam, 1990).
[3] R. Jullien, P. Jund, and D. Caprion, Phys. Rev. E **54**, 6035 (1996).
[4] R. Jullien and P. Meakin, Europhys. Lett. **6**, 629 (1988).
[5] M.P. Allen and D.J. Tildesley, *Computer Simulation of Liquids* (Oxford Science Publications, New York, 1997).
[6] S. Luding, in *Physics of Dry Granular Media*, Vol. 350 *NATO Advanced Studies Institute, Series E: Applied Science*, edited by H.J. Herrmann, J.-P. Hovi, and S. Luding (Kluwer Academic, Dordrecht, The Netherlands, 1998), p. 285.
[7] J.J. Moreau, Eur. J. Mech. A/Solids **13**, 93 (1994).
[8] M. Jean, in *Mechanics of Geometrical Interfaces*, edited by A.P.S. Selvaduri and M. J. Boulon (Elsevier, Amsterdam, 1995), p. 463.
[9] F. Radjai, Comput. Phys. Commun. **121-122**, 294 (1999).
[10] J. Schäfer, S. Dippel, and D.E. Wolf, J. Phys. I **6**, 5 (1996).
[11] P.K. Watson, H. Mizes, A. Castellanos, and A. Mizes, in *Powders and Grains 97*, edited by R.P. Behringer and J. T. Jenkins (Balkema, Rotterdam, 1997), p. 109.
[12] P. Meakin and R. Jullien, J. Phys. (Paris) **46**, 1543 (1985).
[13] M.J. Vold, J. Colloid Sci. **14**, 168 (1959); J. Phys. Chem. **63**, 1608 (1959); **64**, 1616 (1960).
[14] B.D. Lubachevsky, V. Privman, and S.C. Roy, Phys. Rev. E **47**, 48 (1993).
[15] C. Tang and S. Liang, Phys. Rev. Lett. **71**, 2769 (1993).
[16] W.M. Visscher and M. Bolsterli, Nature (London) **239**, 504 (1972).
[17] T.I. Quickenden and G.K. Tan, J. Colloid Interface Sci. **48**, 382 (1974).
[18] F. Radjai and S. Roux, Phys. Rev. E **51**, 6177 (1995).
[19] F. Radjai, J. Schäfer, S. Dippel, and D. Wolf, J. Phys. I **7**, 1053 (1997).
[20] J.G. Berryman, Phys. Rev. A **27**, 1053 (1983).
[21] A. Gervois and D. Bideau, in *Disorder and Granular Media*, edited by D. Bideau and A. Hansen (North-Holland, Amsterdam, 1993), p. 1.
[22] M. Satake, in *Continuum-Mechanical and Statistical Approaches in the Mechanics of Granular Materials*, edited by S.C. Cowin and M. Satake (Gakujutsu Bunken Fukyu-kai, Tokyo, 1978), p. 47–62.
[23] F. Radjai, D. Wolf, M. Jean, and J.J. Moreau, Phys. Rev. Lett. **90**, 61 (1998).
[24] L. Rothenburg and R.J. Bathurst, Géotechnique **39**, 601 (1989).

.

URN:NBN:no-3475